Stability analysis of decoupled time-stepping schemes for the specialized conduction system/myocardium coupled problem in cardiology

Salwa Aouadi, W Mbarki, Nejib Zemzemi

Stability analysis of decoupled time-stepping schemes for the specialized conduction system/myocardium coupled problem in cardiology

S. Aouadi[a], **W. Mbarki**[a] **N. Zemzemi**[b1]

[a] Université Tunis El Manar.
FST 2092 Tunis. Tunisia.
[b] INRIA Bordeaux Sud-Ouest, Carmen project
200 rue de la vieille tour 33405 Talence Cedex, France

Abstract. The Purkinje network is the rapid conduction system in the heart. It ensures the physiological spread of the electrical wave in the ventricles. In this work, we first prove the stability of the space semi-discretized problem. Then we present four different strategies for solving the Purkinje/ myocardium coupled. The strategies are based on different time discretization of the coupling terms. The first scheme is fully coupled, where the coupling terms are considered implicit. The second and the third schemes are based on Gauss-Seidel time-splitting schemes where one coupling term is considered explicit and the other is implicit. The last is a Jacobi-like time-splitting scheme where both coupling terms are considered explicit. Our main result is the proof of the stability of the three considered schemes under the same restriction on the time step. Moreover, we show that the energy of the problem is slightly affected by the time-splitting schemes. We illustrate the theoretical result by different numerical simulations in 2D. We also conduct 3D simulations using physiologically detailed ionic models.

Key words: Cardiac electrophysiology, reaction-diffusion, Purkinje network, myocardium, stability analysis, monodomain, finite element, coupling problem.

AMS subject classification: 12A34, 56B78,35K57, 35K55

[1]Corresponding author. E-mail: nejib.zemzemi@inria.fr

1. Introduction

The excitation of the cardiac cells starts at the sinoatrial node where pacemaker cells generate an electrical current. This current propagates to the right atria then to the left atria through the Bachmann's bundle. The electrical wave does not propagate directly to the ventricle since the interface between the atria and ventricles is insolating. Only the atrioventricular node allows the propagation of this wave to the ventricles. Then the electrical wave follows the His bundle which is a rapid conductive system that ends in the Purkinje fibers directly connected to the ventricular cells. This rapid conduction system is electrically insulated from the heart muscle except at the endpoints that are connected to the myocardium in an area called "Purkinje Muscle Junctions" (PMJ) [3, 6, 34]. A schematic representation of the specialized conduction system both in the atria and the ventricles is given in Figure 1. Many of arrhythmias are related to the His-Purkinje system like in the Wolff-Parkinson-white syndrome where the electrical signal can enter into the different regions of the myocardium. This causes the propagation of two wave fronts at the same time, one from Purkinje to the myocardium and the other in the opposite direction [37]. Also, the left and the right bundle branch block. This leads to a delayed activation of the ventricles[12, 18, 27, 20]. The arrhythmia may also be generated by Ionic effects within the rapid conduction system [7]. Most of the models associated with the specialized conduction system use the monodomain equation. These models consider the Purkinje system as a one dimensional network without worrying about the extracellular part of these bundles. They lead to a non-linear reaction diffusion equations coupled to an ordinary differential equation modelling the ionic activity in cardiac cells [21, 5, 1, 31]. Several studies concerning the modelling of the action potential were held,

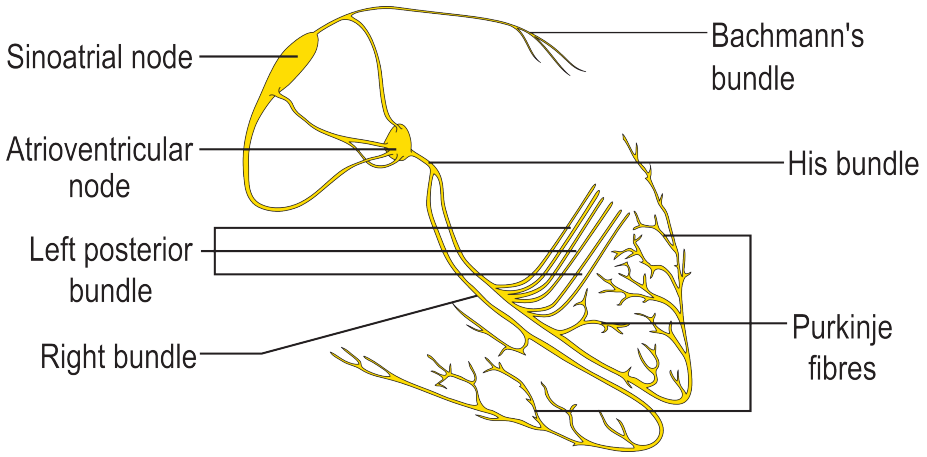

Figure 1: Schematic representation of the specialized conduction system both in the ventricles (His bundle and purkinje fibers) and the atria (Bachmann's bundle). Figure courtesy: Wikipedia. `https://en.wikipedia.org/wiki/Bundle_of_His`

we distinguish the physiological model [28, 4, 10, 22, 23, 33] and the phenomenological

model [14, 26, 30, 2, 25]. In this paper, we will work with both physiological and phenomenological models. For the stability analysis and some numerical results, we will use phenomenological models and for the physiological numerical results, we use the Ten Tusscher model [33] for the 3D geometry and Difrancesco-Noble [10] for the Purkinje network.

In different studies, the Purkinje system has been modeled using the monodomain equation [21, 31, 1, 5]. In order to introduce a physiologically accurate model of the electrical activity of the heart, one should take into account this rapid conductive system and the way it is coupled to the myocardium. Three works have presented different coupling models [36, 3, 6]: In [36], the coupling between the Purkinje cells and the myocardium is represented at the discrete level for the bidomain equation. A mathematical analysis of this representation could not be performed since the coupling conditions are not given in the continuous level. In [3], authors provide a mathematical representation of the coupling conditions at the continuous level, the effect of the Purkinje on the myocardium is represented by a source term. Whereas, the counter effect is based on a robin-like boundary condition on the terminals of the Purkinje network. This representation would be detailed in this paper, as it would be used for the stability analysis that we will perform. In the paper by Bordas *et.al* [6], the coupling of the Purkinje and the myocardium is performed using the bidomain equation for both Purkinje and myocardium. The idea is based on previews work by D'Angelo and Quarteroni [9], where they proposed a reaction-diffusion equation 1D/3D coupling model for an application in tissue perfusion. The model by Bordas *et.al* [6] is derived using an averaging through the cross section of the Purkinje network and by passing to the limit from a cylindrical shape of the Purkinje network to the one dimensional model. A mathematical analysis of the existence and uniqueness of the solution has been provided in the same paper. In the present work, we consider the coupling conditions derived in [3] where the myocardium and Purkinje electrical activities are represented by the monodomain model and are coupled using source terms and Robin boundary conditions. The stability analysis of the monodomain model has been subject of different studies: In [16], authors present a mathematical analysis of a finite difference for solving the monodomain equation coupled to the Beeler-Reuter ionic Model [4] with homogeneous Dirichlet conditions on the boundary of the spatial domain. They also prove the convergence of the numerical and some bounds properties for the action potential, concentrations and gate variables. In [8], authors study the stability and the convergence of a finite volume method for solving the monodomain models coupled to FitzHugh-Nagumo like ionic model [14, 2] with homogeneous Neumann boundary conditions on the boundary of the domain. They also prove a maximum principle property for the action potential variable. This property has been used later for the study of the stability and convergence of the finite volume method. To the best of our knowledge, no work has been dedicated to studying the stability of the purkinje/myocardium coupled problem. The purpose of the paper is two folds: First, our aim is to prove the stability of the finite element method for solving the coupled problem. Second, by detailing the fully discretized problem we raise up some properties of the left-hand side (LHS) matrix and

we show how some time-stepping numerical schemes allow ameliorating the LHS of the fully discretized problem. The main difficulty in using a fully coupled problem is that the LHS matrix of the fully discretized problem is non-symmetric. Using a time stepping scheme would allow solving the two monodomain problems: one in the myocardium and the other the Purkinje network sequentially. Thus both of LHS matrices would be symmetric positive definite.

The model is described in section 2. In section 3., we prove the stability of the space semi-discretized problem using finite elements method. The main contribution is presented In section 4.: We study the stability of the fully discretized problem for the different numerical schemes (Gauss-Seidel and Jacobi uncoupling schemes) by combining different techniques using energy based stability [11, 13] and some theoretical results developed in [17, 35]. We also provide, in section 4., details about the numerical implementation of the four numerical schemes. In the section 5., we conduct some numerical simulations for the 1D/2D and 1D/3D coupled problem using the different time marching schemes and we compare their accuracy.

2. Modelling

Let us denote by $\Omega \subset \mathbb{R}^3$ the myocardium domain, Λ stands for the Purkinje network domain. We suppose that we have N_{ter} terminals in the Purkinje network $(x_1, ..., x_{N_{\text{ter}}})$. Each terminal of the Purkinje is coupled to the myocardium in a small subdomain $\Omega_i \subset \Omega$ called a Purkinje muscle junction (PMJ) (see Figure 2).

We also consider that the Purkinje network Λ is made of a set of disjoint branches $\{\Lambda_i\}_{i=1}^{N^{\text{bran}}}$, where $\Lambda = \cup_{i=1}^{N^{\text{bran}}} \Lambda_i$ and N^{bran} is the number of branches. The boundary of each branch is either a terminal point or a branching node. Let's consider $\{y_1, y_2, ..., y_{p^{\text{bran}}}\}$ the set of the Purkinje branching nodes. Each of the branching nodes y_j is a boundary of a set of branches, we denote by I_j the set of these branches indices. We denote by V the transmembrane voltage in the myocardium and V_{p} the transmembrane voltage in the Purkinje network. Since the use of finite element method on a tree-shaped 1D geometry is not standard, we need to distinguish the derivative of V_{p} at the boundary of each branch. For any branching node y_j, $j = 1, \ldots, p^{\text{bran}}$ and for any $k \in I_j$, we denote by $\partial_{x,k} V_{\text{p}}(y_j)$ the derivative V_{p} on the point y_j seen as the boundary of the branch Λ_k.

$$\partial_{x,k} V_{\text{p}}(y_j) = \lim_{\substack{y \to y_j \\ y \in \Lambda_k}} \partial_x V_{\text{p}}(y),$$

where ∂_x is the tangential derivative a long the Purkinje branch. Following this definition, the Kirchhoff law on the branching nodes reads as follows

$$\sum_{k \in I_j} \sigma_{\text{p}} \partial_{x,k} V_{\text{p}}(y_j) = 0, \ \forall j = 1, \ldots, p^{\text{bran}}.$$

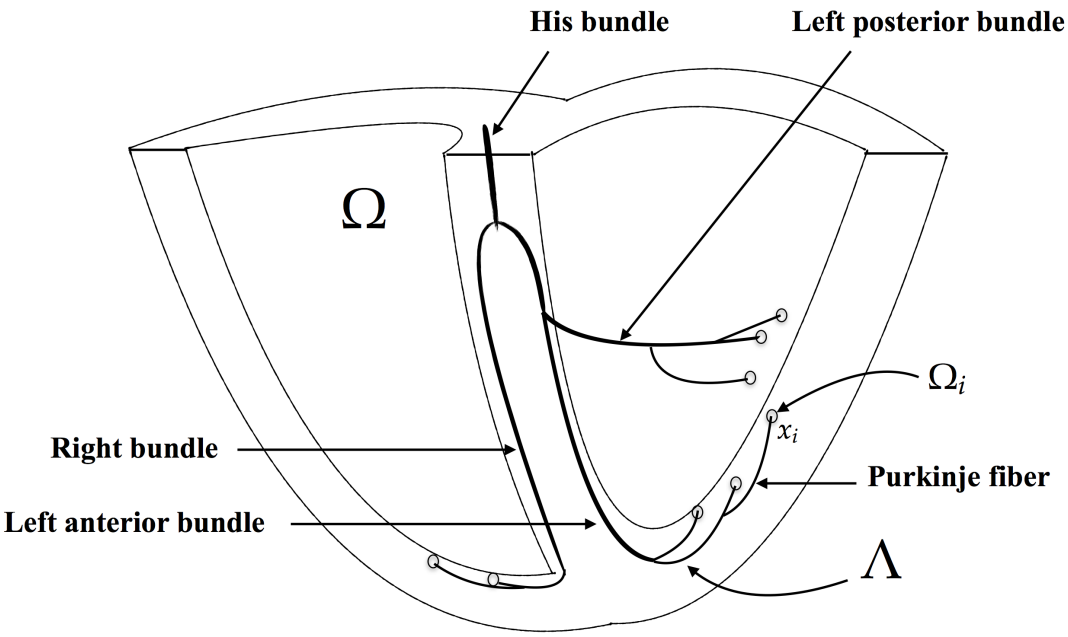

Figure 2: Schematic representation of the 1D/3D coupled problem domains: Λ represents the Purkinje fiber and Hiss, right and left bundles, Ω represents the myocardium and Ω_i is the coupling zone between the Purkinje end node (x_i) and the myocardium.

2.1. PDE model

In the space/time domain $\Omega \times [0, T]$, the electrical wave is governed by the monodomain model [3]: a non-linear reaction diffusion equation and a dynamic system modelling the cellular ionic currents

$$\begin{cases} A(C\partial_t V + I_{\text{ion}}(V, W)) + \sum_{i=2}^{N_{\text{ter}}} s_i = div(\boldsymbol{\sigma}\nabla V) + A\, I_{\text{app}}, \quad in\ \Omega \times [0, T], \\ \partial_t W + g(V, W) = 0, \quad in\ \Omega \times [0, T], \\ \boldsymbol{\sigma}\nabla V \cdot \boldsymbol{n} = 0, \ on\ \partial\Omega \times [0, T], \\ V(0, .) = V_0, \quad W(0, .) = W_0, \ in\ \Omega, \end{cases} \tag{2.1}$$

The last equation in (2.1), means that the heart is supposed to be insulated. The electrical wave in the Purkinje system is also governed by the monodomain equation

$$\begin{cases} A_{\mathrm{p}}(C_{\mathrm{p}}\partial_t V_{\mathrm{p}} + I_{\mathrm{ion,p}}(V_{\mathrm{p}}, W_{\mathrm{p}})) = div(\boldsymbol{\sigma}_{\mathrm{p}}\nabla V_{\mathrm{p}})) + A_{\mathrm{p}} I_{\mathrm{app,p}}, \ \ on\ \Lambda \times [0,T], \\ \sum_{k\in I_j} \boldsymbol{\sigma}_{\mathrm{p}}\partial_{x,k} V_{\mathrm{p}}(y_j) = 0,\ \forall j = 1,\dots,p^{\mathrm{bran}}, \\ \boldsymbol{\sigma}_{\mathrm{p}}\partial_x V_{\mathrm{p}}(x) = 0,\ \ for\ x = x_1\ on\ [0,T], \\ \partial_t W_{\mathrm{p}} + g_{\mathrm{p}}(V_{\mathrm{p}}, W_{\mathrm{p}}) = 0, \ \ on\ \Lambda \times [0,T]. \\ V_{\mathrm{p}}(0,.) = V_{\mathrm{p},0}, \quad W_{\mathrm{p}}(0,.) = W_{\mathrm{p},0}, \ \ in\ \Lambda. \end{cases} \tag{2.2}$$

In the myocardium Ω (respectively Purkinje network Λ), constant A (respectively, A_{p}) represents the surface of membrane per unit of volume, C (respectively, C_{p}) is the capacitance of the cell membrane, I_{app} (respectively, $I_{\mathrm{app,p}}$) the applied current, I_{ion} (respectively, $I_{\mathrm{ion,p}}$) is the total ionic current, W (respectively, W_{p}) represents the ionic model state variables it could include concentrations of different ionic entities and gating variable. In this study, the dynamics of W, W_{p}, I_{ion} and $I_{\mathrm{ion,p}}$ are described by phenomenological two state-variable models introduced that will be presented bellow. Electrical conductivities in both domains are given $\boldsymbol{\sigma}$ in the myocardium and $\boldsymbol{\sigma}_{\mathrm{p}}$ in the Purkinje network. At the heart boundary, $\boldsymbol{n}$ stands for the outward unit normal on $\partial\Omega$. The third equation in (2.2), means that the Purkinje system is insulated at (x_1), the location of the atrioventricular node. Functions V_0, W_0, $V_{\mathrm{p},0}$ and $W_{\mathrm{p},0}$ are the initial conditions of the system.

Following [3], the source current ($\sum_{i=2}^{N_{\mathrm{ter}}} s_i$) flowing from the Purkinje system to the myocardium represents the electrical effect of Purkinje on the myocardium, the counter effect is given by a robin boundary condition as follows

$$\begin{cases} \boldsymbol{\sigma}_{\mathrm{p}}(x_i)\partial_x V_{\mathrm{p}}(x_i) = \dfrac{c_{\mathrm{p}}}{S_{\mathrm{p}}}(\langle V\rangle_i - V_{\mathrm{p}}(x_i)) \text{ for } i = 2,...,N_{\mathrm{ter}}, \\ s_i(x) = \begin{cases} s_i := \frac{S_{\mathrm{p}}}{|\Omega_i|}\boldsymbol{\sigma}_{\mathrm{p}}(x_i)\partial_x V_{\mathrm{p}}(x_i) & if x \in \Omega_i \\ 0 & else \end{cases} \text{ for } i = 2,..,N_{\mathrm{ter}}, \end{cases} \tag{2.3}$$

where, $\langle V\rangle_i = \frac{1}{\Omega_i}\int_{\Omega_i} V$, for $i = 1,...N_{\mathrm{ter}}$, c_{p} the conductance of the PMJ, S_{p} the surface of membrane of the Purkinje cells in Ω_i.

2.2. Ionic models

The generic definition of I_{ion}, $I_{\mathrm{ion,p}}$ g and g_{p} for each of the phenomenological ionic models are given as follows

- FitzHugh-Nagumo (FHN)

$$I_{ion}(V,W) = -f(V,W) = V(V-1)(V-a) + W, \qquad g(V,W) = kV - W, \tag{2.4}$$

  where parameters a and k statisfie $0 < a < 1$ and $k > 0$.

- Rogers-McCulloc (RM)

$$I_{ion}(V,W) = -f(V,W) = V(V-1)(V-a) + VW, \qquad g(V,W) = kV - W, \tag{2.5}$$

where parameters a and k statisfie $0 < a < 1$ and $k > 0$.

- Aliev Panfilov (AP)

$$I_{ion}(V,W) = -f(V,W) = kV(V-1)(V-a) + VW, \qquad g(V,W) = kV(1+a-V) - W, \tag{2.6}$$

- Mitchell-Scheaffer (MS)

$$I_{\text{ion}}(V,W) = \frac{W}{\tau_{in}}V^2(V-1) + \frac{V}{\tau_{out}}, \quad g(V,W) = \begin{cases} \dfrac{W-1}{\tau_{open}}, & \text{if } V \leqslant V_{gate}, \\ \dfrac{W}{\tau_{close}}, & \text{if } V > V_{gate}, \end{cases} \tag{2.7}$$

where the values of the parameters $\tau_{in}, \tau_{out}, \tau_{open}, \tau_{close}, V_{gate}$ are provided in table 1. These values would be used later for the numerical simulations.

Table 1 Mitchell and Schaeffer ionic model parameters. The time constants τ_{in}, τ_{out}, τ_{open}, τ_{close} are in millisecond and V_{gate} is in millivolt.

τ_{in}	τ_{out}	τ_{open}	τ_{close}	V_{gate}
0.3	6	120	150	0.12

In what follows, we refer to FitzHugh-Nagumo like models any of the FHN, RM and AP models. The existence and the uniqueness of a solution for the monodomain problem using these models could be found in [8]. For the existence of a solution for the monodomain problem coupled to the MS model, the proof is much more technical because of the non-local lipshitzianity of the function g when $V = V_{gate}$. A recent work by Kunish and Marica [19] provides the proof and the regularity of solutions using Filippov theory and compactness techniques.

2.3. Regularity of the solution

Assumption 1: We suppose that $\Omega \subset R^d$ $(d = 3, 2)$ has a C^2 regular boundary $\partial\Omega$, the conductivity tensor $\boldsymbol{\sigma} \in C^1\left(\bar{\Omega}, \mathbb{R}^{d\times d}\right)$, $\sigma_{\text{p}} \in C^1\left(\bar{\Lambda}, \mathbb{R}\right)$ and there exist positive constants $\underline{\sigma}$, $\bar{\sigma}$ $\underline{\sigma_{\text{p}}}$, $\bar{\sigma_{\text{p}}}$ such that $\forall \xi \in \mathbb{R}^3$, $\rho \in \mathbb{R}$ we have

$$\begin{aligned} &\underline{\sigma} \parallel \xi \parallel_{l^2}^2 \leq \xi^T \boldsymbol{\sigma}(x)\xi \leq \bar{\sigma} \parallel \xi \parallel_{l^2}^2, \quad \forall\, x \in \Omega, \\ &\underline{\sigma_{\text{p}}}\rho^2 \leq \sigma_{\text{p}}(x)\rho^2 \leq \bar{\sigma_{\text{p}}}\rho^2, \quad \forall\, x \in \Lambda. \end{aligned} \tag{2.8}$$

Theorem 1. *Let $T > 0$, let $V_{\mathrm{p},0} \in H^2(\Lambda)$, $V_0 \in H^2(\Omega)$, $W_{\mathrm{p},0} \in L^\infty(\Lambda)$, $W_0 \in L^\infty(\Omega)$, $I_{\mathrm{app}} \in L^\infty(\Omega)$ and $I_{\mathrm{app,p}} \in L^2(\Lambda)$ be given data and let conductivity tensors satisfy **Assumption 1**, then the Cauchy problem* (2.1)-(2.3) *has a unique solution and the mapping $t \mapsto (V(t,.), V_{\mathrm{p}}(t,.), W(t,.), W_{\mathrm{p}}(t,.))$ is continuous in $H^2(\Omega)\times H^2(\Lambda)\times L^\infty(\Omega)\times L^\infty(\Lambda)$. Moreover, we have*

$$\left(V, V_{\mathrm{p}}, W, W_{\mathrm{p}}\right) \in L^\infty([0,T]\times\Omega)\times L^\infty([0,T]\times\Lambda)\times L^\infty([0,T]\times\Omega)\times L^\infty([0,T]\times\Lambda).$$

The proof of this theorem follows the same arguments used in [32, 8] for the FHN-like ionic models and [19] for the MS model. In what follows, we will make use the following corollary for the proof of the semi-discretized and fully discretized problem stability

Corollary 2. *Assuming the assumptions of **Theorem 1**, we have*

$$\begin{aligned} I_{\mathrm{ion}}(V,W) &\le C_I(|V|+|W|) \qquad I_{\mathrm{ion},p}(V_{\mathrm{p}},W_{\mathrm{p}}) \le C_{i,\mathrm{p}}(|V_{\mathrm{p}}|+|W_{\mathrm{p}}|) \\ g(V,W) &\le C_g(|V|+|W|) \qquad g_{\mathrm{p}}(V_{\mathrm{p}},W_{\mathrm{p}}) \le C_{g,p}(|V_{\mathrm{p}}|+|W_{\mathrm{p}}|). \end{aligned} \tag{2.9}$$

Here, constants C_I, C_g are different from $C_{i,\mathrm{p}}, C_{g,p}$ because we suppose that some ionic parameters could be different in Purkinje and the myocardium models. This property is satisfied for the solutions of the coupled problem because of the $L^\infty([0,T]\times\Omega)$ (respectively, $L^\infty([0,T]\times\Lambda)$.) for V and W (respectively, for V_{p} and W_{p}). These properties of the ionic model functions has been used also in [11, 13] as an assumption when dealing with the bidomain equation.

3. Stability analysis of the semi-discretized problem

Lemma 3..1. ***(Gronwall's lemma)***
let $\beta \in \mathbb{R}$, $\phi \in C^1([0,T],\mathbb{R})$ and $f \in C^0([0,T],\mathbb{R})$ with

$$d_t\phi \le \beta\phi + f,$$

then

$$\forall t \in [0,T], \qquad \phi(t) \le e^{\beta t}\phi(0) + \int_0^t e^{\beta(t-s)} f(s)ds. \tag{3.1}$$

3.1. Space discretization

We first introduce a spatial semi-discretization of the monodomain model through first order Lagrange finite elements.
The variational formulation of the coupled problem (2.1)- (2.3) reads as follows:

Find, for each $t \in]0,T[$,
$(V, V_\mathrm{p}, W, W_\mathrm{p}) \in H^2(\Omega) \times H^2(\Lambda) \times L^2(\Omega) \times L^2(\Lambda)$, such that

$$
\begin{cases}
A(C \displaystyle\int_\Omega \partial_t V \Phi + I_\mathrm{ion}(V,W)\Phi) + \sum_{i=2}^{N_\mathrm{ter}} \int_\Omega s_i \Phi + \int_\Omega \boldsymbol{\sigma} \nabla V \cdot \nabla \Phi - \int_\Omega A\, I_\mathrm{app} \Phi \ = 0, \ \forall \Phi \in H^2(\Omega), \\
\displaystyle\int_\Omega \partial_t W \Psi + \int_\Omega g(V,W)\Psi = 0, \ \forall \Psi \in L^2(\Omega), \\
A_\mathrm{p}(C_\mathrm{p} \displaystyle\int_\Lambda \partial_t V_\mathrm{p} \Phi_\mathrm{p} + I_\mathrm{ion,p}(V_\mathrm{p}, W_\mathrm{p})\Phi_\mathrm{p}) + \int_\Lambda \boldsymbol{\sigma}_\mathrm{p} \nabla V_\mathrm{p} \cdot \nabla \Phi_\mathrm{p} - \sum_{i=2}^{N_\mathrm{ter}} \frac{c_\mathrm{p}}{S_\mathrm{p}} (\langle V \rangle_i - V_\mathrm{p}(x_i)) \Phi_\mathrm{p}(x_i) \\
\qquad\qquad -A_\mathrm{p} \displaystyle\int_\Lambda I_\mathrm{app,p} \Phi_\mathrm{p} = 0, \ \forall\, \Phi_\mathrm{p} \in H^2(\Lambda) \\
\displaystyle\int_\Lambda \partial_t W_\mathrm{p} \Psi_\mathrm{p} + \int_\Lambda g_\mathrm{p}(V_\mathrm{p}, W_\mathrm{p}) \Psi_\mathrm{p} = 0, \ \forall \Psi_\mathrm{p} \in L^2(\Lambda),
\end{cases}
\tag{3.2}
$$

Let us assume that the domain Ω (resp. Λ) can be covered by a regular partition τ (resp. τ_p) of simplexes triangles (resp. *edges*) of maximal diameter h (resp. h_p) , with N (resp. N_p) nodes, noted x_1 to x_N (resp. $x_{\mathrm{p},1}$ to $x_{\mathrm{p},N_\mathrm{p}}$). Consider the space P^1_h (resp. $P^1_{h_\mathrm{p}}$) of continuous linear finite elements on τ (resp. τ_p) and the usual basis of hat functions $\Phi^h_1, ..., \Phi^h_N$ (resp. $\Phi^{h_\mathrm{p}}_1, ..., \Phi^{h_\mathrm{p}}_{N_\mathrm{p}}$) attached to the nodes $x_1, ..., x_N$ (resp. $x_{\mathrm{p},1}, ..., x_{\mathrm{p},N_\mathrm{p}}$), respectively. The semi-discrete monodomain problem then reads as: find a $(V_h, W_h, V_{\mathrm{p},h}, W_{\mathrm{p},h}) \in \mathscr{C}([0,T]; P^1_h)^2 \times \mathscr{C}([0,T]; P^1_{h_\mathrm{p}})^2$ solution of the following variational equations:

$$
\begin{cases}
A(C \displaystyle\int_\Omega \partial_t V_h \Phi^h_j + I_\mathrm{ion}(V_h, W_h)\Phi^h_j) + \sum_{i=2}^{N_\mathrm{ter}} \int_\Omega s_i \Phi^h_j + \int_\Omega \boldsymbol{\sigma} \nabla V_h \cdot \nabla \Phi^h_j - A \int_\Omega I_\mathrm{app} \Phi^h_j \ = 0 \\
\displaystyle\int_\Omega \partial_t W_h \Phi^h_j + \int_\Omega g(V_h, W_h)\Phi^h_j = 0 \\
A_\mathrm{p}(C_\mathrm{p} \displaystyle\int_\Lambda \partial_t V_{\mathrm{p},h} \Phi^{h,\mathrm{p}}_l + I_\mathrm{ion,p}(V_{\mathrm{p},h}, W_{\mathrm{p},h})\Phi^{h,\mathrm{p}}_l) + \int_\Lambda \boldsymbol{\sigma}_\mathrm{p} \nabla V_{\mathrm{p},h} \cdot \nabla \Phi^{h,\mathrm{p}}_l \\
\qquad\qquad -\displaystyle\sum_{i=2}^{N_\mathrm{ter}} \frac{c_\mathrm{p}}{S_\mathrm{p}} (\langle V_h \rangle_i - V_{\mathrm{p},h}(x_i)) \Phi^{h,\mathrm{p}}_l(x_i) - A_\mathrm{p} \displaystyle\int_\Lambda I_\mathrm{app,p} \Phi^{h,\mathrm{p}}_l = 0 \\
\displaystyle\int_\Lambda \partial_t W_{\mathrm{p},h} \Phi^{h,\mathrm{p}}_l + \int_\Lambda g_\mathrm{p}(V_{\mathrm{p},h}, W_{\mathrm{p},h}) \Phi^{h,\mathrm{p}}_l = 0
\end{cases}
\tag{3.3}
$$

for all $1 = 0, ..., N$ and $1 = 0, ..., N_{\mathrm{p}}$.
In the stability analysis below, we shall make use of the following standard discrete trace-inverse inequality (see [35].)

Lemma 3..2. ***Trace inverse inequality***
We define X_h as an internal continuous Lagrange finite element approximation of $H^1(\Omega)$. Then

$$\| V_h \|^2_{0,\partial\Omega} \leq C_{tr} h^{-1} \|V_h\|^2_{0,\Omega}, \quad \forall V_h \in X_h. \tag{3.4}$$

where C_{tr} a positive constant independent of the discretization parameter h (but that might depend on the polynomial order).

In the proof of the following theorem we will use the trace inverse inequality for finite element space $X_h = P^1_{h_{\mathrm{p}}}$

Theorem 3. *Let $T > 0$, $\lambda > 0$ and let $V_{\mathrm{p},h}(0,.) \in H^2(\Lambda)$, $V_h(0,.) \in H^2(\Omega)$, $W_{\mathrm{p},h}(0,.) \in L^\infty(\Lambda)$, $W_h(0,.) \in L^\infty(\Omega)$, $I_{\mathrm{app}} \in L^2([0,T] \times \Omega)$ and $I_{\mathrm{app,p}} \in L^2([0,T] \times \Lambda)$ be given data and let $(V_h, V_{\mathrm{p},h}, W_h, W_{\mathrm{p},h})$ be a solution of problem* (3.3) *. Assume that Assumptions 1 holds, then*

$$\max_{t\in[0,T]} \Big[\|V_h(t)\|^2_{0,\Omega} + \|V_{\mathrm{p},h}(t)\|^2_{0,\Lambda} + \|W_h(t)\|^2_{0,\Omega} + \|W_{\mathrm{p},h}(t)\|^2_{0,\Lambda} \Big] \leq e^{(\lambda T)} \Big[\|V_h(0)\|^2_{0,\Omega} + \|V_{\mathrm{p},h}(0)\|^2_{0,\Lambda}$$

$$+ \|W_h(0)\|^2_{0,\Omega} + \|W_{\mathrm{p},h}(0)\|^2_{0,\Lambda} \Big] + \frac{1}{\lambda} e^{\lambda T} [1 - e^{-\lambda T}] \Big(\frac{1}{C} \|I_{\mathrm{app}}\|^2_{0,\Omega} + \frac{1}{C_{\mathrm{p}}} \|I_{\mathrm{app,p}}\|^2_{0,\Lambda} \Big)$$

Proof. Using as test functions $\Phi^h_j = V_h$(respectively, $\Phi^h_j = W_h$) in $(3.3)_1$, (respectively, in $(3.3)_2$) and $\Phi^{h,\mathrm{p}}_l = V_{\mathrm{p},h}$ (respectively, $\Phi^{h,\mathrm{p}}_l = W_{\mathrm{p},h}$) in $(3.3)_3$, (respectively, in $(3.3)_4$), and by summing the four equations we obtain

$$\int_\Omega \frac{\partial_t (V_h^2)}{2} + \int_\Omega \frac{\partial_t (W_h^2)}{2} + \int_\Lambda \frac{\partial_t V^2_{\mathrm{p},h})}{2} + \int_\Lambda \frac{\partial_t (W^2_{\mathrm{p},h})}{2} + \underbrace{\frac{1}{AC} \int_\Omega \boldsymbol{\sigma} \nabla V_h \cdot \nabla V_h + \frac{1}{A_{\mathrm{p}} C_{\mathrm{p}}} \int_\Lambda \boldsymbol{\sigma}_{\mathrm{p}} \nabla V_{\mathrm{p},h} \cdot \nabla V_{\mathrm{p},h}}_{I_1}$$

$$= \underbrace{-\frac{1}{C} I_{\mathrm{ion}}(V_h, W_h) V_h - \frac{1}{C_{\mathrm{p}}} I_{\mathrm{ion},p}(V_{\mathrm{p},h}, W_{\mathrm{p},h}) V_{\mathrm{p},h} - \int_\Omega g(V_h, W_h) W_h - \int_\Lambda g_{\mathrm{p}}(V_{\mathrm{p},h}, W_{\mathrm{p},h}) W_{\mathrm{p},h}}_{I_2}$$

$$\underbrace{-\frac{1}{AC} \sum_{i=2}^{N_{\mathrm{ter}}} \int_\Omega \frac{S_{\mathrm{p}}}{|\Omega_i|} \boldsymbol{\sigma}_{\mathrm{p}}(x_i) \partial_x V_{\mathrm{p},h}(x_i) V_h}_{I_3} + \underbrace{\frac{1}{A_{\mathrm{p}} C_{\mathrm{p}}} \sum_{i=2}^{N_{\mathrm{ter}}} \frac{c_{\mathrm{p}}}{S_{\mathrm{p}}} (\langle V_h \rangle_i - V_{\mathrm{p},h}(x_i)) V_{\mathrm{p},h}(x_i)}_{I_4} + \int_\Omega \frac{I_{\mathrm{app}}}{C} V_h + \int_\Lambda \frac{I_{\mathrm{app,p}}}{C_{\mathrm{p}}} V_{\mathrm{p},h}$$

(3.5)

Using the lower bound for the eigenvalues of the conductivity tensor we obtain

$$I_1 = \frac{1}{AC}\int_\Omega \boldsymbol{\sigma}\nabla V_h \cdot \nabla V_h + \frac{1}{A_\mathrm{p}C_\mathrm{p}}\int_\Lambda \boldsymbol{\sigma}_\mathrm{p}\nabla V_{\mathrm{p},h}\cdot\nabla V_{\mathrm{p},h} \geq m_1(|V_h|^2_{1,\Omega} + |V_{\mathrm{p},h}|^2_{1,\Lambda}), \tag{3.6}$$

where $m_1 = \min(\frac{\sigma}{AC}, \frac{\sigma_\mathrm{p}}{A_\mathrm{p}C_\mathrm{p}})$. On the other hand, using the **Corollary 2** on the ionic model, we have

$$\begin{aligned} I_2 =& -\frac{1}{C}\int_\Omega I_{\mathrm{ion}}(V_h, W_h)V_h - \frac{1}{C_\mathrm{p}}\int_\Lambda I_{\mathrm{ion},p}(V_{\mathrm{p},h}, W_{\mathrm{p},h})V_{\mathrm{p},h} - \int_\Omega g(V_h, W_h)W_h - \int_\Lambda g_\mathrm{p}(V_{\mathrm{p},h}, W_{\mathrm{p},h})W_{\mathrm{p},h} \\ &\leq \frac{1}{2C}\int_\Omega (I_{\mathrm{ion}}(V_h, W_h))^2 + V_h^2 + \frac{1}{2C}\int_\Lambda (I_{\mathrm{ion}}(V_{\mathrm{p},h}, W_{\mathrm{p},h}))^2 + V_{\mathrm{p},h}^2 + \frac{1}{2}\int_\Omega (g(V_h, W_h))^2 + W_h^2 \\ &+ \frac{1}{2}\int_\Lambda (g_\mathrm{p}(V_{\mathrm{p},h}, W_{\mathrm{p},h}))^2 + W_{\mathrm{p},h}^2 \\ &\leq (m_2 + m_4)[\|V_h\|^2_{0,\Omega} + \|W_h\|^2_{0,\Omega}] + (m_3 + m_5)[\|V_{\mathrm{p},h}\|^2_{0,\Lambda} + \|W_{\mathrm{p},h}\|^2_{0,\Lambda}] \end{aligned} \tag{3.7}$$

where $m_2 = \max(\frac{2C_I^2+1}{2C}, \frac{C_I^2}{C})$, $m_3 = \max(\frac{2C_{i,\mathrm{p}}^2+1}{2C_\mathrm{p}}, \frac{C_{i,\mathrm{p}}^2}{C_\mathrm{p}})$, $m_4 = (C_g^2 + \frac{1}{2})$ and $m_5 = (C_{g,p}^2 + \frac{1}{2})$.

For the coupling equation in the myocardium domain, we treat the source term using the trace inverse inequality as follows,

$$\begin{aligned} I_3 = -\sum_{i=2}^{N_\mathrm{ter}} \frac{1}{AC}\int_\Omega \frac{S_\mathrm{p}}{|\Omega_i|}\sigma_\mathrm{p}(x_i)\partial_x V_{\mathrm{p},h}(x_i)\mathbb{1}_{\Omega_i}V_h &\leq \frac{1}{AC}\sum_{i=2}^{N_\mathrm{ter}}\int_\Omega \frac{S_\mathrm{p}}{|\Omega_i|}\sigma_\mathrm{p}(x_i)\partial_x V_{\mathrm{p},h}(x_i)\mathbb{1}_{\Omega_i}V_h \\ &\leq \frac{m_6}{2}\Big[\sum_{i=2}^{N_\mathrm{ter}}\int_{\Omega_i} |\partial_x V_{\mathrm{p},h}(x_i)|^2 + |V_h(x)|^2 dx\Big] \\ &\leq \frac{N_\mathrm{ter}m_6}{2}\Big[\frac{C_\mathrm{tr}}{h}\|V_{\mathrm{p},h}\|^2_{0,\Lambda} + \|V_h\|^2_{0,\Omega}\Big] \\ &\leq m_7\Big[\|V_{\mathrm{p},h}\|^2_{0,\Lambda} + \|V_h\|^2_{0,\Omega}\Big] \end{aligned} \tag{3.8}$$

where $m_6 = \frac{1}{AC}S_\mathrm{p}\,\bar{\sigma_\mathrm{p}}$ and $m_7 = N_\mathrm{ter}\max(\frac{m_6}{2}\frac{C_\mathrm{tr}}{h}, \frac{m_6}{2})$.

We treat the Robin boundary condition appearing as a coupling condition in the

Purkinje fiber equation as follows,

$$\begin{aligned} I_4 &= \frac{1}{A_{\mathrm{p}}C_{\mathrm{p}}}\sum_{i=2}^{N_{\mathrm{ter}}}\frac{c_{\mathrm{p}}}{S_{\mathrm{p}}}\Big[\langle V_h\rangle_i - V_{\mathrm{p},h}(x_i)\Big]V_{\mathrm{p},h}(x_i) \\ &\leq \frac{c_{\mathrm{p}}}{S_{\mathrm{p}}A_{\mathrm{p}}C_{\mathrm{p}}}\sum_{i=2}^{N_{\mathrm{ter}}}\langle V_h\rangle_i V_{\mathrm{p},h}(x_i) \\ &\leq \frac{c_{\mathrm{p}}}{2S_{\mathrm{p}}A_{\mathrm{p}}C_{\mathrm{p}}\min\{|\Omega_i|\}_{i=2}^{N_{\mathrm{ter}}}}\sum_{i=2}^{N_{\mathrm{ter}}}\|V_h\|^2_{0,\Omega_i} + \frac{c_{\mathrm{p}}}{2S_{\mathrm{p}}A_{\mathrm{p}}C_{\mathrm{p}}}\sum_{i=2}^{N_{\mathrm{ter}}}|V_{\mathrm{p},h}(x_i)|^2 \\ &\leq \frac{c_{\mathrm{p}}}{2S_{\mathrm{p}}A_{\mathrm{p}}C_{\mathrm{p}}\min\{|\Omega_i|\}_{i=2}^{N_{\mathrm{ter}}}}\|V_h\|^2_{0,\Omega} + \frac{C_{\mathrm{tr}}c_{\mathrm{p}}}{2S_{\mathrm{p}}A_{\mathrm{p}}C_{\mathrm{p}}}\frac{1}{h}\|V_{\mathrm{p},h}\|^2_{0,\Lambda}. \\ &\leq m_8\Big[\|V_h\|^2_{0,\Omega} + \|V_{\mathrm{p},h}\|^2_{0,\Lambda}\Big] \end{aligned} \tag{3.9}$$

where $m_8 = \dfrac{c_{\mathrm{p}}}{2S_{\mathrm{p}}A_{\mathrm{p}}C_{\mathrm{p}}}\max\Big(\dfrac{1}{\min\{|\Omega_i|\}_{i=1}^{N_{\mathrm{ter}}}}, \dfrac{C_{\mathrm{tr}}}{h}\Big)$.

Using the inequalities (3.6)-(3.9) and using the Cauchy-Schwarz inequality for the applied current terms I_{app} and $I_{\mathrm{app,p}}$, we obtain:

$$\frac{d}{dt}[\|V_h\|^2_{0,\Omega} + \|V_{\mathrm{p},h}\|^2_{0,\Lambda} + \|W_h\|^2_{0,\Omega} + \|W_{\mathrm{p},h}\|^2_{0,\Lambda}] + 2m_1(|V_h|^2_{1,\Omega} + |V_{\mathrm{p},h}|^2_{1,\Lambda})$$

$$\leq \lambda[\|V_h\|^2_{0,\Omega} + \|V_{\mathrm{p},h}\|^2_{0,\Lambda} + \|W_h\|^2_{0,\Omega} + \|W_{\mathrm{p},h}\|^2_{0,\Lambda}] + \frac{1}{C}\|I_{\mathrm{app}}\|^2_{0,\Omega} + \frac{1}{C_{\mathrm{p}}}\|I_{\mathrm{app,p}}\|^2_{0,\Lambda}$$

with $\lambda = 2(\max(m_2 + m_4, m_3 + m_5) + m_7 + m_8 + \frac{1}{2A_{\mathrm{p}}C_{\mathrm{p}}} + \frac{1}{2AC})$.
Applying the Gronwall's lemma gives

$$[\|V_h(t)\|^2_{0,\Omega} + \|V_{\mathrm{p},h}(t)\|^2_{0,\Lambda} + \|W_h(t)\|^2_{0,\Omega} + \|W_{\mathrm{p},h}(t)\|^2_{0,\Lambda}] \leq e^{(\lambda t)}[\|V_h(0)\|^2_{0,\Omega} + \|V_{\mathrm{p},h}(0)\|^2_{0,\Lambda} + \|W_h(0)\|^2_{0,\Omega}$$

$$+\|W_{\mathrm{p},h}(0)\|^2_{0,\Lambda}] - \int_0^t e^{(\lambda(t-s))}[2m(|V_h|^2_1 + |V_{\mathrm{p},h}|^2_1) - (\frac{1}{C}\|I_{\mathrm{app}}\|^2_{0,\Omega} + \frac{1}{C_{\mathrm{p}}}\|I_{\mathrm{app,p}}\|^2_{0,\Lambda})]ds.$$

Hence,

$$\max_{t\in[0,T]}[\|V_h(t)\|^2_{0,\Omega} + \|V_{\mathrm{p},h}(t)\|^2_{0,\Lambda} + \|W_h(t)\|^2_{0,\Omega} + \|W_{\mathrm{p},h}(t)\|^2_{0,\Lambda}] \leq e^{(\lambda T)}[\|V_h(0)\|^2_{0,\Omega} + \|V_{\mathrm{p},h}(0)\|^2_{0,\Lambda} + \|W_h(0)\|^2_{0,\Omega}$$

$$+\|W_{\mathrm{p},h}(0)\|^2_{0,\Lambda}] + \frac{1}{\lambda}e^{\lambda T}[1 - e^{-\lambda T}](\frac{1}{C}\|I_{\mathrm{app}}\|^2_{0,\Omega} + \frac{1}{C_{\mathrm{p}}}\|I_{\mathrm{app,p}}\|^2_{0,\Lambda})$$

□

4. Stability of the full discretized problem

In this section, we present the space discretization and the different time-splitting schemes we will be using for solving the Purkinje myocardium coupled problem. In the stability analysis below, we shall make use of the following discrete Gronwall's lemma (see [17]).

Lemma 4..1. ***Discret Gronwall's lemma***
let k, B and a_l, b_l, c_l, γ_l, for integers $l \geq 0$, be non-negative numbers such that:

$$a_n + k\sum_{l=0}^{n} b_l \leq k\sum_{l=0}^{n} \gamma_l a_l + k\sum_{l=0}^{n} c_l + B \quad for\ n \geq 0,$$

suppose that $k\gamma_l < 1$, for all l, and set $\sigma_l = (1 - k\gamma_l)^{-1}$. Then,

$$a_n + k\sum_{l=0}^{n} b_l \leq \exp\Big(k\sum_{l=0}^{n} \sigma_l\gamma_l\Big)\Big\{k\sum_{l=0}^{n} c_l + B\Big\}\ for\ n \geq 0. \tag{4.1}$$

4.1. Time discretization

First we present the time discretization of the variational formulation of the Purkinje myocardium coupled problem. For the sake of simplicity, we use a first order semi-implicit time discretization.

$$\begin{cases} A(C\int_\Omega (V_h^{n+1} - V_h^n)\phi + \Delta t\int_\Omega I_{\text{ion}}(V_h^n, W_h^{n+1})\phi) - \Delta t A\int_\Omega I_{\text{app}}^{n+1}\phi \\ \qquad +\Delta t\sum_{i=2}^{N_{\text{ter}}}\int_\Omega \frac{S_{\text{p}}}{|\Omega_i|}\boldsymbol{\sigma}_{\text{p}}(x_i)\partial_x V_{\text{p},h}^{\star}(x_i)\mathbb{1}_{\Omega_i}\phi + \Delta t\int_\Omega \boldsymbol{\sigma}\nabla V_h^{n+1}\cdot\nabla\phi \ = 0 \quad \forall\phi \in L^2(\Omega) \\ \\ \int_\Omega (W_h^{n+1} - W_h^n)\psi + \Delta t\int_\Omega g(V_h^n, W_h^{n+1})\psi = 0 \quad \forall\psi \in L^2(\Omega) \\ \\ A_{\text{p}}(C_{\text{p}}\int_\Lambda (V_{\text{p},h}^{n+1} - V_{\text{p},h}^n)\phi_{\text{p}} + \Delta t\int_\Lambda I_{\text{ion,p}}(V_{\text{p},h}^n, W_{\text{p},h}^{n+1})\phi_{\text{p}}) - \Delta t A_{\text{p}}\int_\Lambda I_{\text{app,p}}^{n+1}\phi_{\text{p}} \\ \qquad +\Delta t\int_\Lambda \boldsymbol{\sigma}\nabla V_{\text{p},h}^{n+1}\cdot\nabla\phi_{\text{p}} + \sum_{i=2}^{N_{\text{ter}}}\frac{c_{\text{p}}\Delta t}{|\Omega_i|A_{\text{p}}C_{\text{p}}}(V_{\text{p},h}^{n+1}(x_i) - \langle V_h^{\star}\rangle_i)\phi_{\text{p}}(x_i) \ = 0 \quad \forall\phi_{\text{p}} \in H^2(\Lambda) \\ \\ \int_\Lambda (W_{\text{p},h}^{n+1} - W_{\text{p},h}^n)\psi_{\text{p}} + \Delta t\int_\Lambda g_{\text{p}}(V_{\text{p},h}^n, W_{\text{p},h}^{n+1})\psi_{\text{p}} = 0 \quad \forall\psi_{\text{p}} \in L^2(\Lambda) \end{cases} \tag{4.2}$$

Depending the choice of $V_h^{\star}$ and $V_{\text{p},h}^{\star}$, where $(^{\star})$ could be $(^n)$ or $(^{n+1})$, we can allow a full coupling or different time-splitting schemes solving the coupled problem.

- Full coupling: $(V_h^\star, V_{\mathrm{p},h}^\star) = (V_h^{n+1}, V_{\mathrm{p},h}^{n+1})$
  The coupling conditions could be introduced implicitly using a full coupling scheme as follows equation (4.3). This means that equation (2.1)-(2.2)-(2.3) are solved in the same system. This could be expensive when using refined meshes.
  Both of the coupling conditions, robin boundary condition and the source term s_i, are introduced in the first member of the linear system:

$$\begin{cases} s_i^{n+1} = \dfrac{S_{\mathrm{p}}\sigma_{\mathrm{p}}(x_i)}{|\Omega_i|h}(V_{\mathrm{p},h}^{n+1}(x_i) - V_{\mathrm{p},h}^{n+1}(x_{i-1})), \text{ for } i = 2, ..., N_{\mathrm{ter}} \\ V_{\mathrm{p},h}^{n+1}(x_i)[1 + \dfrac{c_{\mathrm{p}}h}{S_{\mathrm{p}}\sigma_{\mathrm{p}}(x_i)}] - V_{\mathrm{p},h}^{n+1}(x_{i-1}) = \dfrac{c_{\mathrm{p}}h}{S_{\mathrm{p}}\sigma_{\mathrm{p}}(x_i)}\langle V_h^{n+1}\rangle_i, \text{ for } i = 2, ..., N_{\mathrm{ter}}. \end{cases} \tag{4.3}$$

  h is the space step. In the next paragraph, we propose different time-splitting schemes applied to equation (3) in order to uncouple equation (1) from equation (2). We distinguish tow types of time-splitting methods: Gauss-Seidel like and Jacobi like numerical schemes.

- Gauss-Seidel Purkinje to myocardium (P→M) scheme: $(V_h^\star, V_{\mathrm{p},h}^\star) = (V_h^n, V_{\mathrm{p},h}^{n+1})$
  We first compute the solution on the Purkinje system using the average of the myocardial potential at the previous time step, then we compute the myocardial potential using the solution of the Purkinje system.
  The coupling conditions are then discretized as follows:

$$\begin{cases} V_{\mathrm{p},h}^{n+1}(x_i)[1 + \dfrac{c_{\mathrm{p}}h}{S_{\mathrm{p}}\sigma_{\mathrm{p}}(x_i)}] - V_{\mathrm{p},h}^{n+1}(x_{i-1}) = \dfrac{c_{\mathrm{p}}h}{S_{\mathrm{p}}\sigma_{\mathrm{p}}(x_i)}\langle V_h^{n}\rangle_i, \text{ for } i = 2, ..., N_{\mathrm{ter}}, \\ s_i^{n+1} = \dfrac{S_{\mathrm{p}}\sigma_{\mathrm{p}}(x_i)}{|\Omega_i|h}(V_{\mathrm{p},h}^{n+1}(x_i) - V_{\mathrm{p},h}^{n+1}(x_{i-1})), \text{ for } i = 2, ..., N_{\mathrm{ter}}. \end{cases} \tag{4.4}$$

- Gauss-Seidel myocardium to Purkinje (M→P) scheme: $(V_h^\star, V_{\mathrm{p},h}^\star) = (V_h^{n+1}, V_{\mathrm{p},h}^{n})$
  We first compute the myocardial potential using the solution of the Purkinje system at the previous time step, then we compute the solution of the Purkinje system using the average of the myocardial potential.
  The coupling conditions are then discretized as follows:

$$\begin{cases} s_i^{n+1} = \dfrac{S_{\mathrm{p}}\sigma_{\mathrm{p}}(x_i)}{|\Omega_i|h}(V_{\mathrm{p},h}^{n}(x_i) - V_{\mathrm{p},h}^{n}(x_{i-1})), \text{ for } i = 2, ..., N_{\mathrm{ter}}, \\ V_{\mathrm{p},h}^{n+1}(x_i)[1 + \dfrac{c_{\mathrm{p}}h}{S_{\mathrm{p}}\sigma_{\mathrm{p}}(x_i)}] - V_{\mathrm{p},h}^{n+1}(x_{i-1}) = \dfrac{c_{\mathrm{p}}h}{S_{\mathrm{p}}\sigma_{\mathrm{p}}(x_i)}\langle V_h^{n+1}\rangle_i, \text{ for } i = 2, ..., N_{\mathrm{ter}}. \end{cases} \tag{4.5}$$

- Jacobi scheme: $(V_h^\star, V_{\mathrm{p},h}^\star) = (V_h^n, V_{\mathrm{p},h}^n)$
  We compute the myocardial potential using the solution of the Purkinje system at the previous time step, and we compute the solution of the Purkinje system using

the average of the myocardial potential at the previous time step.
The coupling conditions are then discretized as follows:

$$\begin{cases} s_i^{n+1} = \dfrac{S_{\rm p}\boldsymbol{\sigma}_{\rm p}(x_i)}{|\Omega_i|h}(V_{{\rm p},h}^n(x_i) - V_{{\rm p},h}^n(x_{i-1})), \text{ for } i = 2, ..., N_{\rm ter}, \\ V_{{\rm p},h}^{n+1}(x_i)[1 + \dfrac{c_{\rm p}h}{S_{\rm p}\boldsymbol{\sigma}_{\rm p}(x_i)}] - V_{{\rm p},h}^{n+1}(x_{i-1}) = \dfrac{c_{\rm p}h}{S_{\rm p}\boldsymbol{\sigma}_{\rm p}(x_i)}\langle V_h^n\rangle_i, \text{ for } i = 2, ..., N_{\rm ter}. \end{cases} \tag{4.6}$$

4.2. Stability of the time-splitting schemes

Our main result concerns the energy based stability of the fully discretized myocardium/Purkinje coupled problem. Let us first denote by

$$a_m \stackrel{\rm def}{=} \|V_h^m\|_{0,\Omega}^2 + \|V_{{\rm p},h}^m\|_{0,\Lambda}^2 + \|W_h^m\|_{0,\Omega}^2 + \|W_{{\rm p},h}^m\|_{0,\Lambda}^2,$$

$$a_0 = \|V_h^0\|_{0,\Omega}^2 + \|V_{{\rm p},h}^0\|_{0,\Lambda}^2 + \|W_h^0\|_{0,\Omega}^2 + \|W_{{\rm p},h}^0\|_{0,\Lambda}^2,$$

$$b_n = \|\nabla V_{{\rm p},h}^n\|_{0,\Lambda}^2 + \|\nabla V_h^n\|_{0,\Omega}^2,$$

and the energy

$$E_m \stackrel{\rm def}{=} a_m + \Delta t \sum_{n=0}^{m} \left(\|\nabla V_{{\rm p},h}^n\|_{0,\Lambda}^2 + \|\nabla V_h^n\|_{0,\Omega}^2\right)$$

Theorem 4. *Let $m\Delta t = T > 0$, $V_{{\rm p},h}(0) \in H^2(\Lambda)$, $V_h(0) \in H^2(\Omega)$, $W_{{\rm p},h}(0) \in L^2(\Lambda)$, $W_h(0) \in L^2(\Omega)$, $I_{\rm app} \in L^2(\Omega)$ and $I_{{\rm app},{\rm p}} \in L^2(\Lambda)$ be given data and let $(V_h^n, V_{{\rm p},h}^n, W_h^n, W_{{\rm p},h}^n)_{n=0}^m$ the solution of problem* (4.2)*. Assume that* ***Assumtion 1,2*** *are satisfied, then for each of the four time marching schemes described above, there exist a constant $C > 0$ and a constant $\gamma > 0$ depending on the parameters of the model, the time T and (h) such that for all*

$$\Delta t < \frac{1}{\gamma} \tag{4.7}$$

we have

$$E_m \le C.$$

Proof. In the system of equations (4.2), we replace the test function $(\phi, \phi_{\rm p}, \psi, \psi_{\rm p})$ by $(V_h^{n+1}, V_{{\rm p},h}^{n+1}, W_h^{n+1}, W_{{\rm p},h}^{n+1})$. By summing the four equations and using the identity

$$2(a^{n+1} - a^n)a^{n+1} = (a^{n+1})^2 + (a^{n+1} - a^n)^2 - (a^n)^2,$$

we obtain,

$$
\begin{aligned}
&\|V_h^{n+1}\|_{0,\Omega}^2 + \|V_h^{n+1} - V_h^n\|_{0,\Omega}^2 - \|V_h^n\|_{0,\Omega}^2 + \|V_{\mathrm{p},h}^{n+1}\|_{0,\Lambda}^2 + \|V_{\mathrm{p},h}^{n+1} - V_{\mathrm{p},h}^n\|_{0,\Lambda}^2 - \|V_{\mathrm{p},h}^n\|_{0,\Lambda}^2 + \|W_h^{n+1}\|_{0,\Omega}^2 \\
&+ \|W_h^{n+1} - W_h^n\|_{0,\Omega}^2 - \|W_h^n\|_{0,\Omega}^2 + \|W_{\mathrm{p},h}^{n+1}\|_{0,\Lambda}^2 + \|W_{\mathrm{p},h}^{n+1} - W_{\mathrm{p},h}^n\|_{0,\Lambda}^2 - \|W_{\mathrm{p},h}^n\|_{0,\Lambda}^2 + \frac{2\Delta t}{AC}\int_\Omega \sigma|\nabla V_h^{n+1}|^2 \\
&+ \frac{2\Delta t}{A_{\mathrm{p}}C_{\mathrm{p}}}\int_\Lambda \sigma_{\mathrm{p}}|\nabla V_{\mathrm{p},h}^{n+1}|^2 \\
&= \underbrace{-\frac{2\Delta t}{C}\int_\Omega I_{\mathrm{ion}}(V_h^n, W_h^{n+1})V_h^{n+1}}_{J_1} \underbrace{-\frac{2\Delta t}{C_{\mathrm{p}}}\int_\Lambda I_{\mathrm{ion,p}}(V_{\mathrm{p},h}^n, W_{\mathrm{p},h}^{n+1})V_{\mathrm{p},h}^{n+1}}_{J_2} \underbrace{-2\Delta t\int_\Omega g(V_h^n, W_h^{n+1})W_h^{n+1}}_{J_3} \\
&\underbrace{-2\Delta t\int_\Lambda g_{\mathrm{p}}(V_{\mathrm{p},h}^n, W_{\mathrm{p},h}^{n+1})W_{\mathrm{p},h}^{n+1}}_{J_4} \underbrace{-\frac{2\Delta t}{AC}\sum_{i=2}^{N_{\mathrm{ter}}}\int_\Omega \frac{S_{\mathrm{p}}}{|\Omega_i|}\sigma_{\mathrm{p}}(x_i)\partial_x V_{\mathrm{p},h}^\star(x_i)\mathbb{1}_{\Omega_i}V_h^{n+1}}_{J_5} + \frac{2\Delta t}{C_{\mathrm{p}}}\int_\Lambda I_{\mathrm{app,p}}^{n+1}V_{\mathrm{p},h}^{n+1} \\
&+ \frac{2\Delta t}{C}\int_\Omega I_{\mathrm{app}}^{n+1}V_h^{n+1} + \underbrace{\sum_{i=2}^{N_{\mathrm{ter}}}\frac{2c_{\mathrm{p}}\Delta t}{S_{\mathrm{p}}A_{\mathrm{p}}C_{\mathrm{p}}}(\langle V_h^\star\rangle_i - V_{\mathrm{p},h}^{n+1}(x_i))V_{\mathrm{p},h}^{n+1}(x_i)}_{J_6}
\end{aligned}
$$

Using the **Corollary 2** we have

$$
\begin{aligned}
J_1 = -\frac{2\Delta t}{C}\int_\Omega I_{\mathrm{ion}}(V_h^n, W_h^{n+1})V_h^{n+1} &\le \frac{\Delta t}{C}\Big(\int_\Omega I_{\mathrm{ion}}^2(V_h^n, W_h^{n+1}) + \int_\Omega (V_h^{n+1})^2\Big) \\
&\le \frac{2\Delta t C_I^2}{C}(\|V_h^n\|_{0,\Omega}^2 + \|W_h^{n+1}\|_{0,\Omega}^2) + \frac{\Delta t}{C}\|V_h^{n+1}\|_{0,\Omega}^2
\end{aligned}
\tag{4.8}
$$

Similarly,

$$
\begin{aligned}
J_2 = -\frac{2\Delta t}{C_{\mathrm{p}}}\int_\Lambda I_{\mathrm{ion,p}}(V_{\mathrm{p},h}^n, W_{\mathrm{p},h}^{n+1})V_{\mathrm{p},h}^{n+1} &\le \frac{\Delta t}{C_{\mathrm{p}}}\Big(\int_\Lambda I_{\mathrm{ion,p}}^2(V_{\mathrm{p},h}^n, W_{\mathrm{p},h}^{n+1}) + \int_\Lambda (V_{\mathrm{p},h}^{n+1})^2\Big) \\
&\le \frac{2\Delta t C_{i,\mathrm{p}}^2}{C_{\mathrm{p}}}(\|V_{\mathrm{p},h}^n\|_{0,\Lambda}^2 + \|W_{\mathrm{p},h}^{n+1}\|_{0,\Lambda}^2) + \frac{\Delta t}{C_{\mathrm{p}}}\|V_{\mathrm{p},h}^{n+1}\|_{0,\Lambda}^2
\end{aligned}
\tag{4.9}
$$

Also using the **Corollary 2** we obtain for the right hand side of the cell variable,

$$
\begin{aligned}
J_3 = -2\Delta t\int_\Omega g(V_h^n, W_h^{n+1})W_h^{n+1} &\le \Delta t\Big(\int_\Omega g^2(V_h^n, W_h^{n+1}) + \int_\Omega (W_h^{n+1})^2\Big) \\
&\le 2\Delta t C_g^2(\|V_h^n\|_{0,\Omega}^2 + \|W_h^{n+1}\|_{0,\Omega}^2) + \Delta t\|W_h^{n+1}\|_{0,\Omega}^2
\end{aligned}
\tag{4.10}
$$

$$
\begin{aligned}
J_4 = -2\Delta t\int_\Lambda g(V_{\mathrm{p},h}^n, W_{\mathrm{p},h}^{n+1})W_{\mathrm{p},h}^{n+1} &\le \Delta t\Big(\int_\Lambda (g_{\mathrm{p}}(V_{\mathrm{p},h}^n, W_{\mathrm{p},h}^{n+1}))^2 + \int_\Lambda (W_{\mathrm{p},h}^{n+1})^2\Big) \\
&\le 2\Delta t C_{g_{\mathrm{p}}}^2(\|V_{\mathrm{p},h}^n\|_{0,\Lambda}^2 + \|W_{\mathrm{p},h}^{n+1}\|_{0,\Lambda}^2) + \Delta t\|W_{\mathrm{p},h}^{n+1}\|_{0,\Lambda}^2.
\end{aligned}
\tag{4.11}
$$

For the coupling condition that appears as a source term in the myocardium domain, we have

$$\begin{aligned} J_5 = -\sum_{i=2}^{N_{\text{ter}}} \frac{2\Delta t}{AC} \int_\Omega \frac{S_{\text{p}}}{|\Omega_i|} \sigma_{\text{p}}(x_i) \partial_x V^\star_{\text{p},h}(x_i) \mathbb{1}_{\Omega_i} V^{n+1}_h &\leq \sum_{i=2}^{N_{\text{ter}}} \frac{2\Delta t S_{\text{p}} \bar{\sigma_{\text{p}}}}{AC|\Omega_i|} \Big[\int_{\Omega_i} |\partial_x V^\star_{\text{p},h}(x_i)| |V^{n+1}_h| \Big] \\ &\leq \frac{2\Delta t S_{\text{p}} \bar{\sigma_{\text{p}}}}{AC \min\{|\Omega_i|\}_{i=2}^{N_{\text{ter}}}} \sum_{i=2}^{N_{\text{ter}}} \Big[\int_{\Omega_i} |\partial_x V^\star_{\text{p},h}(x_i)| |V^{n+1}_h| \Big] \\ &\leq \frac{2\Delta t S_{\text{p}} \bar{\sigma_{\text{p}}}}{AC \min\{|\Omega_i|\}_{i=2}^{N_{\text{ter}}}} \sum_{i=2}^{N_{\text{ter}}} \Big[\int_{\Omega_i} \sqrt{\frac{C_{\text{tr}}}{h}} \|\nabla V^\star_{\text{p},h}\|_{0,\Lambda} |V^{n+1}_h| \Big] \\ &\leq \frac{2\Delta t S_{\text{p}} \bar{\sigma_{\text{p}}}}{AC \min\{|\Omega_i|\}_{i=2}^{N_{\text{ter}}}} \sqrt{\frac{C_{\text{tr}}}{h}} \|\nabla V^\star_{\text{p},h}\|_{0,\Lambda} \sum_{i=2}^{N_{\text{ter}}} \Big[\int_{\Omega_i} |V^{n+1}_h| \Big] \\ &\leq \frac{\Delta t \sigma_{\text{p}}}{A_{\text{p}} C_{\text{p}}} \|\nabla V^\star_{\text{p},h}\|^2_{0,\Lambda} + \frac{\Delta t}{h} \frac{A_{\text{p}} C_{\text{p}} C_{\text{tr}} S_{\text{p}}^2 \bar{\sigma_{\text{p}}}^2}{AC \left(\min\{|\Omega_i|\}_{i=2}^{N_{\text{ter}}} \right)^2 \sigma_{\text{p}}} \|V^{n+1}_h\|^2_{0,\Omega} \end{aligned} \tag{4.12}$$

In order to treat the term J_6, we start by controlling the square of the potential mean value in Ω_i using the Hölder's inequality

$$\begin{aligned} \langle V^\star_h \rangle_i^2 &= \Big(\frac{1}{|\Omega_i|} \int_{\Omega_i} V^\star_h(x) dx \Big)^2 \\ &\leq \frac{1}{|\Omega_i|} \|V^\star_h\|^2_{0,\Omega_i} \end{aligned}$$

Hence we obtain,

$$\begin{aligned} J_6 &= \sum_{i=2}^{N_{\text{ter}}} \frac{2 c_{\text{p}} \Delta t}{S_{\text{p}} A_{\text{p}} C_{\text{p}}} (\langle V^\star_h \rangle_i - V^{n+1}_{\text{p},h}(x_i)) V^{n+1}_{\text{p},h}(x_i) \\ &\leq \sum_{i=2}^{N_{\text{ter}}} \frac{2 c_{\text{p}} \Delta t}{S_{\text{p}} A_{\text{p}} C_{\text{p}}} \langle V^\star_h \rangle_i V^{n+1}_{\text{p},h}(x_i) \\ &\leq \frac{c_{\text{p}} \Delta t}{S_{\text{p}} A_{\text{p}} C_{\text{p}} \min\{|\Omega_i|\}_{i=2}^{N_{\text{ter}}}} \sum_{i=2}^{N_{\text{ter}}} \|V^\star_h\|^2_{0,\Omega_i} + \frac{c_{\text{p}} \Delta t}{S_{\text{p}} A_{\text{p}} C_{\text{p}}} \sum_{i=2}^{N_{\text{ter}}} |V^{n+1}_{\text{p},h}(x_i)|^2 \\ &\leq \frac{c_{\text{p}} \Delta t}{S_{\text{p}} A_{\text{p}} C_{\text{p}} \min\{|\Omega_i|\}_{i=2}^{N_{\text{ter}}}} \|V^\star_h\|^2_{0,\Omega} + \frac{C_{\text{tr}} c_{\text{p}}}{S_{\text{p}} A_{\text{p}} C_{\text{p}}} \frac{\Delta t}{h} \|V^{n+1}_{\text{p},h}\|^2_{0,\Lambda}. \end{aligned} \tag{4.13}$$

On the other hand, we use the Cauchy-Schwarz inequality for the applied current terms,

$$\frac{2\Delta t}{C} \int_\Omega I^{n+1}_{\text{app}} V^{n+1}_h \leq \frac{\Delta t}{C} (\|I^{n+1}_{\text{app}}\|^2_{0,\Omega} + \|V^{n+1}_h\|^2_{0,\Omega})$$

$$\frac{2\Delta t}{C_{\mathrm{p}}}\int_{\Lambda} I_{\mathrm{app,p}}^{n+1} V_{\mathrm{p},h}^{n+1} \leq \frac{\Delta t}{C_{\mathrm{p}}}(\|I_{\mathrm{app,p}}^{n+1}\|_{0,\Lambda}^2 + \|V_{\mathrm{p},h}^{n+1}\|_{0,\Lambda}^2)$$

Using the inequalities (4.8)-(4.13), we obtain

$$\begin{aligned}
&\|V_h^{n+1}\|_{0,\Omega}^2 + \|V_h^{n+1} - V_h^n\|_{0,\Omega}^2 - \|V_h^n\|_{0,\Omega}^2 + \|V_{\mathrm{p},h}^{n+1}\|_{0,\Lambda}^2 + \|V_{\mathrm{p},h}^{n+1} - V_{\mathrm{p},h}^n\|_{0,\Lambda}^2 - \|V_{\mathrm{p},h}^n\|_{0,\Lambda}^2 + \|W_h^{n+1}\|_{0,\Omega}^2 \\
&+ \|W_h^{n+1} - W_h^n\|_{0,\Omega}^2 - \|W_h^n\|_{0,\Omega}^2 + \|W_{\mathrm{p},h}^{n+1}\|_{0,\Lambda}^2 + \|W_{\mathrm{p},h}^{n+1} - W_{\mathrm{p},h}^n\|_{0,\Lambda}^2 - \|W_{\mathrm{p},h}^n\|_{0,\Lambda}^2 + \Delta t(\alpha_9\|\nabla V_h^{n+1}\|_{0,\Omega}^2 \\
&+ \alpha_{10}\|\nabla V_{\mathrm{p},h}^{n+1}\|_{0,\Lambda}^2) \\
&\leq \Delta t\Big(\alpha_1\|V_h^n\|_{0,\Omega}^2 + \alpha_2\|V_{\mathrm{p},h}^n\|_{0,\Lambda}^2 + \alpha_3\|W_h^{n+1}\|_{0,\Omega}^2 + \alpha_4\|W_{\mathrm{p},h}^{n+1}\|_{0,\Lambda}^2 + \alpha_5\|V_h^{n+1}\|_{0,\Omega}^2 + \alpha_6\|V_{\mathrm{p},h}^{n+1}\|_{0,\Lambda}^2 \\
&+ \alpha_7\|V_h^\star\|_{0,\Omega}^2 + \alpha_8\|\nabla V_{\mathrm{p},h}^\star\|_{0,\Lambda}^2\Big) + \Delta t(\frac{1}{C}\|I_{\mathrm{app}}^{n+1}\|_{0,\Omega}^2 + \frac{1}{C_{\mathrm{p}}}\|I_{\mathrm{app,p}}^{n+1}\|_{0,\Lambda}^2)
\end{aligned} \tag{4.14}$$

where,

$$\alpha_1 = 2(\frac{C_I^2}{C} + C_g^2),\ \alpha_2 = 2(\frac{C_{i,\mathrm{p}}^2}{C_{\mathrm{p}}} + C_{g,p}^2),\ \alpha_3 = (1 + 2C_g^2 + 2\frac{C_I^2}{C}),\ \alpha_4 = (1 + 2C_{g,p}^2 + \frac{C_{i,\mathrm{p}}^2}{C_{\mathrm{p}}})$$

$$\alpha_5 = \frac{1}{C} + \frac{1}{AC} + \frac{A_{\mathrm{p}}C_{\mathrm{p}}C_{\mathrm{tr}}S_{\mathrm{p}}^2\bar{\sigma_{\mathrm{p}}}}{h\,AC\,\left(\min\{|\Omega_i|\}_{i=2}^{N_{\mathrm{ter}}}\right)^2}, \alpha_6 = \frac{1}{C_{\mathrm{p}}} + \frac{1}{A_{\mathrm{p}}C_{\mathrm{p}}} + \frac{C_{\mathrm{tr}}c_{\mathrm{p}}}{hS_{\mathrm{p}}A_{\mathrm{p}}C_{\mathrm{p}}},$$

$$\alpha_7 = \frac{c_{\mathrm{p}}}{S_{\mathrm{p}}A_{\mathrm{p}}C_{\mathrm{p}}\min\{|\Omega_i|\}_{i=2}^{N_{\mathrm{ter}}}},\ \alpha_8 = \frac{\sigma_{\mathrm{p}}}{AC},\ \alpha_9 = \frac{2\underline{\sigma}}{AC},\ \alpha_{10} = \frac{2\sigma_{\mathrm{p}}}{A_{\mathrm{p}}C_{\mathrm{p}}} = 2\alpha_8\,.$$

By summing equation (4.14) over n, $0 \leq n \leq m-1$, we have

$$\|V_h^m\|_{0,\Omega}^2 + \|V_{\mathrm{p},h}^m\|_{0,\Lambda}^2 + \|W_h^m\|_{0,\Omega}^2 + \|W_{\mathrm{p},h}^m\|_{0,\Lambda}^2 - (\|V_h^0\|_{0,\Omega}^2 + \|V_{\mathrm{p},h}^0\|_{0,\Lambda}^2 + \|W_h^0\|_{0,\Omega}^2 + \|W_{\mathrm{p},h}^0\|_{0,\Lambda}^2)$$

$$+\Delta t(\alpha_{10}\sum_{n=0}^{m-1}\|\nabla V_{\mathrm{p},h}^{n+1}\|_{0,\Lambda}^2 + \alpha_9\sum_{n=0}^{m-1}\|\nabla V_h^{n+1}\|_{0,\Omega}^2)$$

$$\leq \Delta t\sum_{n=0}^{m-1}\Big(\alpha_1\|V_h^n\|_{0,\Omega}^2 + \alpha_2\|V_{\mathrm{p},h}^n\|_{0,\Lambda}^2 + \alpha_3\|W_h^{n+1}\|_{0,\Omega}^2 + \alpha_4\|W_{\mathrm{p},h}^{n+1}\|_{0,\Lambda}^2 + \alpha_5\|V_h^{n+1}\|_{0,\Omega}^2 + \alpha_6\|V_{\mathrm{p},h}^{n+1}\|_{0,\Lambda}^2$$

$$+\alpha_7\|V_h^\star\|_{0,\Omega}^2 + \alpha_8\|\nabla V_{\mathrm{p},h}^\star\|_{0,\Lambda}^2\Big) + \Delta t\sum_{n=0}^{m-1}(\frac{1}{C}\|I_{\mathrm{app}}^{n+1}\|_{0,\Omega}^2 + \frac{1}{C_{\mathrm{p}}}\|I_{\mathrm{app,p}}^{n+1}\|_{0,\Lambda}^2)$$

We then obtain

$$a_m + \Delta t(\alpha_{10}\sum_{n=0}^{m-1}\|\nabla V_{\mathrm{p},h}^{n+1}\|_{0,\Lambda}^2 + \alpha_9\sum_{n=0}^{m-1}\|\nabla V_h^{n+1}\|_{0,\Omega}^2) \le \Delta t\sum_{n=0}^{m-1}\Big(\alpha_1\|V_h^n\|_{0,\Omega}^2 + \alpha_2\|V_{\mathrm{p},h}^n\|_{0,\Lambda}^2 + \alpha_3\|W_h^{n+1}\|_{0,\Omega}^2$$
$$+ \alpha_4\|W_{\mathrm{p},h}^{n+1}\|_{0,\Lambda}^2 + \alpha_5\|V_h^{n+1}\|_{0,\Omega}^2 + \alpha_6\|V_{\mathrm{p},h}^{n+1}\|_{0,\Lambda}^2 + \alpha_7\|V_h^\star\|_{0,\Omega}^2 + \alpha_8\|\nabla V_{\mathrm{p},h}^\star\|_{0,\Lambda}^2\Big) + \Delta t\sum_{n=0}^{m-1}(\frac{1}{C}\|, I_{\mathrm{app}}^{n+1}\|_{0,\Omega}^2$$
$$+ \frac{1}{C_{\mathrm{p}}}\|I_{\mathrm{app,p}}^{n+1}\|_{0,\Lambda}^2) + a_0. \tag{4.15}$$

This gives, for instance, in the case of the full coupling $(V_h^\star, V_{\mathrm{p},h}^\star) = (V_h^{n+1}, V_{\mathrm{p},h}^{n+1})$

$$a_m + \Delta t\sum_{n=0}^{m}\Big(\alpha_8\|\nabla V_{\mathrm{p},h}^n\|_{0,\Lambda}^2 + \alpha_9\|\nabla V_h^n\|_{0,\Omega}^2\Big)$$

$$\le \Delta t\sum_{n=0}^{m}\gamma a_n + \Delta t\sum_{n=0}^{m}(\frac{1}{C}\|I_{\mathrm{app}}^n\|_{0,\Omega}^2 + \frac{1}{C_{\mathrm{p}}}\|I_{\mathrm{app,p}}^n\|_{0,\Lambda}^2) + \Delta t[\alpha_8\|\nabla V_{\mathrm{p},h}^0\|_{0,\Lambda}^2 + \alpha_9\|\nabla V_h^0\|_{0,\Omega}^2] + a_0,$$

where $\gamma = \max(\alpha_1 + \alpha_5 + \alpha_7, \alpha_2 + \alpha_6 + \alpha_8, \alpha_3, \alpha_4)$.

Applying the discrete Gronwall's lemma, we obtain the following estimates for each of the proposed numerical schemes:

1. **Full coupling** $(V_h^\star, V_{\mathrm{p},h}^\star) = (V_h^{n+1}, V_{\mathrm{p},h}^{n+1})$

   For all $\Delta t < \frac{1}{\gamma}$ we have

$$a_m + \Delta t\sum_{n=0}^{m}\Big(\alpha_8\|\nabla V_{\mathrm{p},h}^n\|_{0,\Lambda}^2 + \alpha_9\|\nabla V_h^n\|_{0,\Omega}^2\Big) \le C[\Delta t\Big(\sum_{n=0}^{m}(\frac{1}{C}\|I_{\mathrm{app}}^{n+1}\|_{0,\Omega}^2 + \frac{1}{C_{\mathrm{p}}}\|I_{\mathrm{app,p}}^n\|_{0,\Lambda}^2)$$
$$+ \alpha_8\|\nabla V_{\mathrm{p},h}^0\|_{0,\Lambda}^2 + \alpha_9\|\nabla V_h^0\|_{0,\Omega}^2\Big) + a_0].$$

2. **Gauss-Seidel scheme from Purkinje to myocardium (P→M):** $(V_h^\star, V_{\mathrm{p},h}^\star) = (V_h^n, V_{\mathrm{p},h}^{n+1})$
   For all $\Delta t < \frac{1}{\gamma}$ we have

$$a_m + \Delta t\sum_{n=0}^{m}\Big(\alpha_8\|\nabla V_{\mathrm{p},h}^n\|_{0,\Lambda}^2 + \alpha_9\|\nabla V_h^n\|_{0,\Omega}^2\Big) \le C[\Delta t\Big(\sum_{n=0}^{m}(\frac{1}{C}\|I_{\mathrm{app}}^{n+1}\|_{0,\Omega}^2 + \frac{1}{C_{\mathrm{p}}}\|I_{\mathrm{app,p}}^n\|_{0,\Lambda}^2)$$
$$+ \alpha_8\|\nabla V_{\mathrm{p},h}^0\|_{0,\Lambda}^2 + \alpha_9\|\nabla V_h^0\|_{0,\Omega}^2\Big) + a_0].$$

3. **Gauss-Seidel scheme from the myocardium to Purkinje (M→P)**: $(V_h^\star, V_{\mathrm{p},h}^\star) = (V_h^{n+1}, V_{\mathrm{p},h}^n)$
   For all $\Delta t < \frac{1}{\gamma}$ we have

$$a_m + \Delta t \sum_{n=0}^{m} \left(\alpha_8 \|\nabla V_{\mathrm{p},h}^n\|_{0,\Lambda}^2 + \alpha_9 \|\nabla V_h^n\|_{0,\Omega}^2\right) + \Delta t \alpha_8 \|\nabla V_{\mathrm{p},h}^m\|_{0,\Lambda}^2$$
$$\leq C[\Delta t\Big(\sum_{n=0}^{m}(\frac{1}{C}\|I_{\mathrm{app}}^{n+1}\|_{0,\Omega}^2 + \frac{1}{C_{\mathrm{p}}}\|I_{\mathrm{app,p}}^n\|_{0,\Lambda}^2) + \alpha_{10}\|\nabla V_{\mathrm{p},h}^0\|_{0,\Lambda}^2 + \alpha_9\|\nabla V_h^0\|_{0,\Omega}^2\Big) + a_0]$$

4. **Jacobi scheme** $(V_h^\star, V_{\mathrm{p},h}^\star) = (V_h^n, V_{\mathrm{p},h}^n)$
   For all $\Delta t < \frac{1}{\gamma}$ we have

$$a_m + \Delta t \sum_{n=0}^{m} \left(\alpha_8 \|\nabla V_{\mathrm{p},h}^n\|_{0,\Lambda}^2 + \alpha_9 \|\nabla V_h^n\|_{0,\Omega}^2\right) + \Delta t \alpha_8 \|\nabla V_{\mathrm{p},h}^m\|_{0,\Lambda}^2$$
$$\leq C\Big[\Delta t\Big(\sum_{n=0}^{m}(\frac{1}{C}\|I_{\mathrm{app}}^{n+1}\|_{0,\Omega}^2 + \frac{1}{C_{\mathrm{p}}}\|I_{\mathrm{app,p}}^n\|_{0,\Lambda}^2) + \alpha_{10}\|\nabla V_{\mathrm{p},h}^0\|_{0,\Lambda}^2 + \alpha_9\|\nabla V_h^0\|_{0,\Omega}^2\Big) + a_0\Big].$$

The proof of the theorem holds from these refined estimates. □

Remark 4..2. *For a sufficiently small value of h, we could see that* $\gamma = \max(\alpha_1+\alpha_5+\alpha_7, \alpha_2+\alpha_6+\alpha_8)$ *for all the time-splitting schemes. We could also see from* α_5 *and* α_6 *that we have a CFL-like condition* $\Delta t = O((h))$.

Remark 4..3. *In addition, we remark from the expression of* α_5 *that* Δt *depends on the minimal size of the coupling regions* $\min\{|\Omega_i|\}_{i=2}^{N_{\mathrm{ter}}}$. *The smaller is* $\min\{|\Omega_i|\}_{i=2}^{N_{\mathrm{ter}}}$, *the smaller should be* Δt. *In practice coupling regions* $\{\Omega_i\}_{i=2}^{N_{\mathrm{ter}}}$ *are fixed in the geometry.*

Remark 4..4. *The difference in the terms that control the energy for the different schemes are lead by the norm of the gradient of the action potential in the Purkinje domain at the initial condition and the last time step. This means that the energy is controlled by the same expression (* $C\Big[a_0 + \Delta t\Big(\sum_{n=0}^{m}(\frac{1}{C}\|I_{\mathrm{app}}^{n+1}\|_{0,\Omega}^2 + \frac{1}{C_{\mathrm{p}}}\|I_{\mathrm{app,p}}^n\|_{0,\Lambda}^2)\Big)\Big]$ *) when the initial condition is constant.*

4.3. Numerical implementation

In order to show the algorithm we use to solve the Purkinje/myocardium coupled problem, we first introduce the time and space descritization of the state variables. The finite element approximation of $V(t^n)$ in the first order finite element space P_h^1 is approximated by V_h^n as follows

$$V_h^n = \sum_{i=1}^{N} V_{h,i}^n \Phi_i^h.$$

We introduce the finite element approximation of the other state variable in the same way:

$$W_h^n = \sum_{i=1}^{N} W_{h,i}^n \Phi_i^h, \;\; V_{\mathrm{p},h}^n = \sum_{i=1}^{N_p} V_{\mathrm{p},h,i}^n \Phi_i^{h,\mathrm{p}} \text{ and } W_{\mathrm{p},h}^n = \sum_{i=1}^{N_p} W_{\mathrm{p},h,i}^n \Phi_i^{h,\mathrm{p}}.$$

Since W and W_{p} satisfy an ordinary differential equation. We start by solving them point-wise, *i.e* at each node of both myacardium and Purkinje meshes.

$$W_{h,i}^{n+1} - W_{h,i}^n + \Delta t \, g_h(V_{h,i}^n, W_{h,i}^{n+1}) = 0, \text{for } i = 1, \dots, N,$$
$$W_{\mathrm{p},h,i}^{n+1} - W_{\mathrm{p},h,i}^{n+1} + \Delta t \, g_{\mathrm{p}}(V_{\mathrm{p},h,i}^n, W_{\mathrm{p},h,i}^{n+1}) = 0, \text{for } i = 1, \dots, N_{\mathrm{p}}.$$

In the case of the Mitchell and Scheaffer model and since $V_{h,i}^n$ and $V_{\mathrm{p},h,i}^n$ are fixed in the interval $[t^n, t^{n+1}]$, one can use an analytical expression of the solution. Once the solutions $W_{\mathrm{p}}(t^n)$ and $W_{\mathrm{p},h,i}^{n+1}$ are computed. We can explicitly approximate the value of the ionic currents on each node of the mesh. We define the finite element approximation of I_{ion} at time t^{n+1} by $I_{\mathrm{ion},h}^{n+1} = \sum_{i=1}^{N} I_{\mathrm{ion},h,i}^{n+1} \Phi_i$, where $I_{\mathrm{ion},h,i}^{n+1} = I_{\mathrm{ion}}(V_{h,i}^n, W_{h,i}^{n+1})$ for $i = 1, \dots, N$. In the same way, we define $I_{\mathrm{ion,p},h,i}^{n+1} = I_{\mathrm{ion,p}}(V_{\mathrm{p},h,i}^n, W_{\mathrm{p},h,i}^{n+1})$, for $i = 1, \dots, N_{\mathrm{p}}$. The projection of the applied current I_{app} at time t^{n+1} on the finite element space is given by $I_{\mathrm{app},h}^{n+1} = \sum_{i=1}^{N} I_{\mathrm{app},h,i}^{n+1} \Phi_i$, where $I_{\mathrm{app},h,i}^{n+1} = I_{\mathrm{app}}(x_i, t^{n+1})$, for $i = 1, \dots, N$. In the same, we define $I_{\mathrm{app,p},h}^{n+1} = \sum_{i=1}^{N_{\mathrm{p}}} I_{\mathrm{app,p},h,i}^{n+1} \Phi_i$.
Using the fully descritized equation (4.2) we obtain the following linear problem:

$$\begin{cases} \chi(\boldsymbol{M} + \Delta t \, \boldsymbol{K})\boldsymbol{V}_h^{n+1} + \boldsymbol{S}(\boldsymbol{V}_{\mathrm{p},h}^{\star}) = \boldsymbol{V}_h^n + \Delta t \, \boldsymbol{F}_h^{n+1}(\boldsymbol{V}_h^n, \boldsymbol{W}_h^{n+1}) \\ (\chi_{\mathrm{p}} \boldsymbol{M}_{\mathrm{p}} + \Delta t \, \boldsymbol{K}_{\mathrm{p}})\boldsymbol{V}_{\mathrm{p},h}^{n+1} + \boldsymbol{L}(\boldsymbol{V}_h^{\star}) + \boldsymbol{R}\mathrm{obin}(\boldsymbol{V}_{\mathrm{p},h}^{n+1}) = \boldsymbol{V}_{\mathrm{p},h}^n + \Delta t \, \boldsymbol{F}_{\mathrm{p},h}^{n+1}(\boldsymbol{V}_{\mathrm{p},h}^n, W_{\mathrm{p},h}^{n+1}) \end{cases} \tag{4.16}$$

where $\boldsymbol{V}_h^n = [V_{h,1}^n, ..., V_{h,N}^n]^T$, $\boldsymbol{W}_h^n = [W_{h,0}^n, ..., W_{h,N}^n]^T$, $\boldsymbol{V}_{\mathrm{p},h}^n = [V_{\mathrm{p},h,1}^n, ..., V_{\mathrm{p},h,N_p}^n]^T$, $\boldsymbol{W}_{\mathrm{p},h}^n = [W_{\mathrm{p},h,1}^n, ..., W_{\mathrm{p},h,N_p}^n]^T$,.

$$\chi = AC, \quad \boldsymbol{M} = \Big(\int_{\Omega} \Phi_i^h \Phi_j^h\Big)_{i,j=1,\dots,N} \quad , \quad \boldsymbol{K} = \Big(\int_{\Omega} \sigma \nabla \Phi_i^h \nabla \Phi_i^h\Big)_{i,j=1,\dots,N},$$

$$\chi_{\mathrm{p}} = A_{\mathrm{p}} C_{\mathrm{p}}, \;\; \boldsymbol{M}_{\mathrm{p}} = \Big(\int_{\Lambda} \Phi_i^{h,\mathrm{p}} \Phi_j^{h,\mathrm{p}}\Big)_{i,j=1,\dots,N_p} \quad , \quad \boldsymbol{K}_{\mathrm{p}} = \Big(\int_{\Lambda} \sigma_{\mathrm{p}} \nabla \Phi_i^{h,\mathrm{p}} \nabla \Phi_i^{h,\mathrm{p}}\Big)_{i,j=1,\dots,N_p},$$

$\boldsymbol{F}_h^{n+1}(\boldsymbol{V}_h^n, \boldsymbol{W}_h^{n+1}) = \boldsymbol{M}(-A\boldsymbol{I}_{\mathrm{ion},h}^{n+1} + A\boldsymbol{I}_{\mathrm{app},h}^{n+1})$ and $\boldsymbol{F}_{\mathrm{p},h}^{n+1}(\boldsymbol{V}_{\mathrm{p},h}^n, \boldsymbol{W}_{\mathrm{p},h}^{n+1}) = \boldsymbol{M}_{\mathrm{p}}(-A_{\mathrm{p}}\boldsymbol{I}_{\mathrm{ion,p},h}^{n+1} + A_{\mathrm{p}} I_{\mathrm{app,p},h}^{n+1})$.
The non-trivial part concerns the coupling operators $\boldsymbol{S}, \boldsymbol{L}$ and $\boldsymbol{R}$obin. The linear operator $\boldsymbol{S} \in \mathbb{R}^{N \times N_{\mathrm{p}}}$ is a matrix that maps the $V_{\mathrm{p},h}^{\star}$ into the the source current term in the equation (4.2). The linear operation $\boldsymbol{S}(\boldsymbol{V}_{\mathrm{p},h}^{\star})$ represents, in equation (4.2),

$$\begin{aligned} \Delta t \sum_{i=2}^{N_{\mathrm{ter}}} \int_{\Omega} \tfrac{S_{\mathrm{p}}}{|\Omega_i|} \sigma_{\mathrm{p}}(x_i) \partial_x V_{\mathrm{p},h}^{\star}(x_i) \mathbb{1}_{\Omega_i} \phi &= \Delta t \sum_{i=2}^{N_{\mathrm{ter}}} \tfrac{S_{\mathrm{p}}}{|\Omega_i|} \sigma_{\mathrm{p}}(x_i) \partial_x V_{\mathrm{p},h}^{\star}(x_i) \int_{\Omega_i} \phi \\ &= \Delta t \sum_{i=2}^{N_{\mathrm{ter}}} \tfrac{S_{\mathrm{p}}}{|\Omega_i| h} \sigma_{\mathrm{p}}(x_i) (V_{\mathrm{p},h,i}^{\star} - V_{\mathrm{p},h,i-1}^{\star}) \int_{\Omega_i} \phi. \end{aligned} \tag{4.17}$$

Here, we suppose that for every terminal node x_i in the Purkinje one dimensional mesh, x_{i-1} is its neighborhood node. In order to present the algorithm that we use to compute the operator S. Let us first define the matrix $\boldsymbol{M}_i \in \mathbb{R}^{N\times N}$, where $\boldsymbol{M}_i = (\int_{\Omega_i} \Phi_k^h \Phi_l^h)_{k,l=1,\dots,N}$, for $i = 2, \dots, N_{\text{ter}}$. We also need to define the column vector $\mathbb{1} \in \mathbb{R}^N$, where $\mathbb{1}(i) = 1, i = 1, \dots, N$. The operator $\boldsymbol{S}$ is build following Algorithm 1.

Algorithm 1 Construction of the Source term linear Operator

$\boldsymbol{S} \in \mathbb{R}^{N\times N_{\text{p}}}$
$\boldsymbol{S} = 0$
for $i = 2, \dots N_{\text{ter}}$ **do**
  $\boldsymbol{S}_i \in \mathbb{R}^{N\times N_{\text{p}}}$
  $\boldsymbol{S}_i = 0$
  Compute $\boldsymbol{M}_i = (\int_{\Omega_i} \Phi_k^h \Phi_l^h)_{k,l=1,\dots,N}$
  Compute the column vector $\boldsymbol{X}_i = \frac{\Delta t\, \sigma_p\, S_p}{h\, |\Omega_i|} \boldsymbol{M}_i \mathbb{1}$
  $\boldsymbol{S}_i(:, i) = \boldsymbol{X}_i$
  $\boldsymbol{S}_i(:, i-1) = -\boldsymbol{X}_i$
  $\boldsymbol{S} = \boldsymbol{S} + \boldsymbol{S}_i$
end for

The operator $\boldsymbol{L} \in \mathbb{R}^{N_{\text{p}}\times N}$, represents part of the robin boundary conditions allowing the feedback from the myocardium to Purkinje. As shown in equation (4.3), this term could be written as follows

$$V_{\text{p},h}^{n+1}(x_i)[1 + \frac{c_{\text{p}} h}{S_{\text{p}} \boldsymbol{\sigma}_{\text{p}}(x_i)}] - V_{\text{p},h}^{n+1}(x_{i-1}) = \frac{c_{\text{p}} h}{S_{\text{p}} \boldsymbol{\sigma}_{\text{p}}(x_i)} \langle V_h^\star \rangle_i, \text{ for } i = 2, ..., N_{\text{ter}}. \tag{4.18}$$

We construct the matrix $\boldsymbol{L}$ following Algorithm 2. In the implicite case, when $(\boldsymbol{V}_h^\star, \boldsymbol{V}_{\text{p},h}^\star) =$

Algorithm 2 Construction of the Operator L

$\boldsymbol{L} \in \mathbb{R}^{N_{\text{p}}\times N}$
$\boldsymbol{L} = 0$
for $i = 2, \dots N_{\text{ter}}$ **do**
  $\boldsymbol{L}_i \in \mathbb{R}^{N_{\text{p}}\times N}$
  $\boldsymbol{L}_i = 0$
  Compute $\boldsymbol{M}_i = (\int_{\Omega_i} \Phi_k^h \Phi_l^h)_{k,l=1,\dots,N}$
  Compute the row vector $\boldsymbol{Y}_i = \frac{h\, g_p}{S_p\, \sigma_p\, |\Omega_i|} (\mathbb{1}^T) \boldsymbol{M}_i$
  $\boldsymbol{L}_i(i, :) = \boldsymbol{Y}_i$
  $\boldsymbol{L} = \boldsymbol{L} + \boldsymbol{L}_i$
end for

$(\boldsymbol{V}_h^{n+1}, \boldsymbol{V}_{\text{p},h}^{n+1})$, the linear problem to solve is

$$\left(\begin{array}{c|c} \boldsymbol{A}_{\mathrm{m,m}} & \boldsymbol{A}_{\mathrm{m,p}} \\ \hline \boldsymbol{A}_{\mathrm{p,m}} & \boldsymbol{A}_{\mathrm{p,p}} \end{array}\right)\left(\begin{array}{c} \boldsymbol{V}_h^{n+1} \\ \hline \boldsymbol{V}_{\mathrm{p},h}^{n+1} \end{array}\right) = \left(\begin{array}{c} \boldsymbol{V}_h^{n} + \Delta t\, \boldsymbol{F}_h^{n+1}(\boldsymbol{V}_h^{n}, \boldsymbol{W}_h^{n+1}) \\ \hline \boldsymbol{V}_{\mathrm{p},h}^{n} + \Delta t\, \boldsymbol{F}_{\mathrm{p},h}^{n+1}(\boldsymbol{V}_{\mathrm{p},h}^{n}, W_{\mathrm{p},h}^{n+1}) \end{array}\right), \tag{4.19}$$

where, $\boldsymbol{A}_{\mathrm{m,m}} = \chi(\boldsymbol{M} + \Delta t\, \boldsymbol{K})$, $\boldsymbol{A}_{\mathrm{m,p}} = \boldsymbol{S}$ and $\boldsymbol{A}_{\mathrm{p,m}} = \boldsymbol{L}$. The matrix $\boldsymbol{A}_{\mathrm{p,p}}$ is a modification of the matrix $(\chi_{\mathrm{p}}\boldsymbol{M}_{\mathrm{p}} + \Delta t\, \boldsymbol{K}_{\mathrm{p}})$ in order to include the robin boundary conditions. It is computed following Algorithm 3. The robin linear operator used in the system (4.16)

Algorithm 3 Application of robin boundary condition in the Purkinje matrix

$\boldsymbol{A}_{\mathrm{p,p}} \in \mathbb{R}^{N_{\mathrm{p}} \times N_{\mathrm{p}}}$
$\boldsymbol{A}_{\mathrm{p,p}} = (\chi_{\mathrm{p}}\boldsymbol{M}_{\mathrm{p}} + \Delta t\, \boldsymbol{K}_{\mathrm{p}})$
for $i = 2, \ldots N_{\mathrm{ter}}$ **do**
  $\boldsymbol{A}_{\mathrm{p,p}}(i,i) = 1 + \dfrac{h\, g_p}{\sigma_p\, S_p}$
  $\boldsymbol{A}_{\mathrm{p,p}}(i, i-1) = -1$
end for

could be obtained as follows $\boldsymbol{R}\mathrm{obin} = \boldsymbol{A}_{\mathrm{p,p}} - (\chi_{\mathrm{p}}\boldsymbol{M}_{\mathrm{p}} + \Delta t\, \boldsymbol{K}_{\mathrm{p}})$.
For the three other schemes the computation of $\boldsymbol{V}_h^{n+1}$ and $\boldsymbol{V}_{\mathrm{p},h}^{n+}$ are uncoupled.

- Gauss-Seidel myocardium to Purkinje (M→P) scheme: $(\boldsymbol{V}_h^{\star}, \boldsymbol{V}_{\mathrm{p},h}^{\star}) = (\boldsymbol{V}_h^{n+1}, \boldsymbol{V}_{\mathrm{p},h}^{n})$
  First, we solve
  $$\boldsymbol{A}_{\mathrm{m,m}}\boldsymbol{V}_h^{n+1} = \boldsymbol{V}_h^{n} + \boldsymbol{S}\boldsymbol{V}_{\mathrm{p},h}^{n} + \Delta t\, \boldsymbol{F}_h^{n+1}(\boldsymbol{V}_h^{n}, \boldsymbol{W}_h^{n+1}).$$
  Then, we solve
  $$\boldsymbol{A}_{\mathrm{p,p}}\boldsymbol{V}_{\mathrm{p},h}^{n+1} = \boldsymbol{V}_{\mathrm{p},h}^{n} + \boldsymbol{L}\boldsymbol{V}_h^{n+1} + \Delta t\, \boldsymbol{F}_{\mathrm{p},h}^{n+1}(\boldsymbol{V}_{\mathrm{p},h}^{n}, W_{\mathrm{p},h}^{n+1}).$$

- Gauss-Seidel Purkinje to myocardium (P→M) scheme: $(\boldsymbol{V}_h^{\star}, \boldsymbol{V}_{\mathrm{p},h}^{\star}) = (\boldsymbol{V}_h^{n}, \boldsymbol{V}_{\mathrm{p},h}^{n+1})$
  First, we solve
  $$\boldsymbol{A}_{\mathrm{p,p}}\boldsymbol{V}_{\mathrm{p},h}^{n+1} = \boldsymbol{V}_{\mathrm{p},h}^{n} + \boldsymbol{L}\boldsymbol{V}_h^{n} + \Delta t\, \boldsymbol{F}_{\mathrm{p},h}^{n+1}(\boldsymbol{V}_{\mathrm{p},h}^{n}, W_{\mathrm{p},h}^{n+1}).$$
  Then, we solve
  $$\boldsymbol{A}_{\mathrm{m,m}}\boldsymbol{V}_h^{n+1} = \boldsymbol{V}_h^{n} + \boldsymbol{S}\boldsymbol{V}_{\mathrm{p},h}^{n+1} + \Delta t\, \boldsymbol{F}_h^{n+1}(\boldsymbol{V}_h^{n}, \boldsymbol{W}_h^{n+1}).$$

- Jacobi scheme: $(\boldsymbol{V}_h^{\star}, \boldsymbol{V}_{\mathrm{p},h}^{\star}) = (\boldsymbol{V}_h^{n}, \boldsymbol{V}_{\mathrm{p},h}^{n})$
  At the $(n+1)^{\mathrm{th}}$ time iteration, both of the following equations could be solved in parallel
  $$\boldsymbol{A}_{\mathrm{p,p}}\boldsymbol{V}_{\mathrm{p},h}^{n+1} = \boldsymbol{V}_{\mathrm{p},h}^{n} + \boldsymbol{L}\boldsymbol{V}_h^{n} + \Delta t\, \boldsymbol{F}_{\mathrm{p},h}^{n+1}(\boldsymbol{V}_{\mathrm{p},h}^{n}, W_{\mathrm{p},h}^{n+1}),$$
  $$\boldsymbol{A}_{\mathrm{m,m}}\boldsymbol{V}_h^{n+1} = \boldsymbol{V}_h^{n} + \boldsymbol{S}\boldsymbol{V}_{\mathrm{p},h}^{n} + \Delta t\, \boldsymbol{F}_h^{n+1}(\boldsymbol{V}_h^{n}, \boldsymbol{W}_h^{n+1}).$$

5. Numerical results

In this section, we conduct two study cases showing the numerical stability of the different time-splitting schemes presented above. The first case is a 1D/2D coupling, we use this case in order to show the order of convergence of the different numerical schemes. Since we demonstrate the stability analysis with the phenomenological MS ionic model, the results shown in this study case would be performed with the same ionic model. The second case is a 1D/3D coupling problem where we present a realistic 3D heart geometry coupled to a 1D Purkinje system. In this case, we use physiologically detailed transmembrane ionic models both for ventricular and Purkinje cells. Our goal is to show numerically that the stability of different schemes remains true even with physiologically detailed ionic models.

5.1. 1D/2D coupling case: Convergence analysis

In order to illustrate the stability results developed in the previous sections, we conduct here some numerical simulations for the full coupling numerical scheme. The myocardium domain is represented by a square (1 cm x 1 cm) and a first Purkinje fiber is represented by a 1 cm segment.

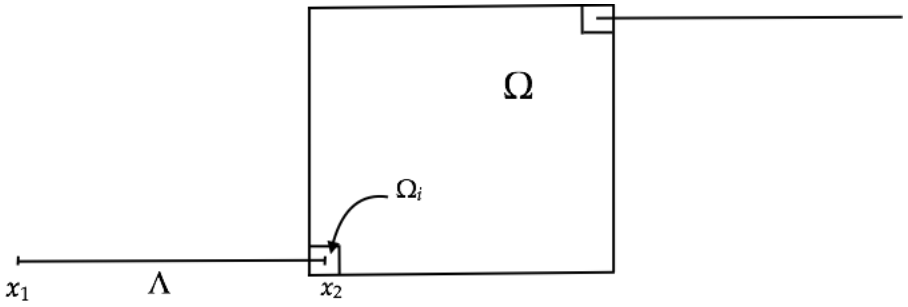

Figure 3: Schematic representation of the 1D/2D coupled problem domains: Λ represents the Purkinje fiber, Ω represents the myocardium and Ω_i is the coupling zone between the Purkinje end node (x_i) and the myocardium. The coupling in the upper right region is similar to the one in the down left region.

The coupling between the Purkinje and the myocardium is performed in the region Ω_i ((0.2 cm x 0.2 cm)) as shown in Figure 3.

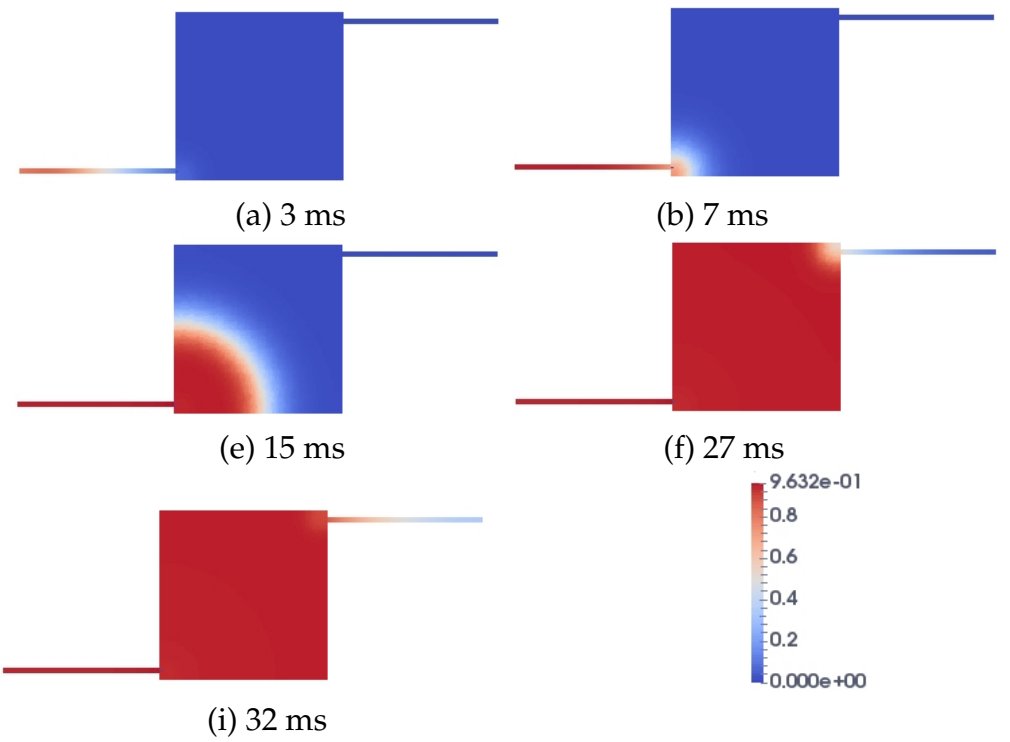

(a) 3 ms (b) 7 ms

(e) 15 ms (f) 27 ms

(i) 32 ms

Figure 4: Snapshots of the depolarization phase of the electrical wave showing the anterograde and retrograde circulation of the electrical wave between Purkinje and myocardium. Simulation are performed with the full coupling scheme.

We also added another segment and coupled it in the top right of the myocardium as shown in Figure 3 the coupling is performed using the same conditions as for the first segment. Our goal is to show that the numerical stability is not affected by the anterograde and retrograde circulation of the current between the Purkinje segment and the myocardium. We stimulate the first segment at its left free extremity. We perform a simulation of the full coupling scheme where space and time discretization parameters are given by $\Delta t = 10^{-2}$ ms $h = 5 \times 10^{-3}$ cm. This simulation would be considered later as the reference solution and would be used for comparison with the time-splitting schemes solutions. In Figure 4, we present the results for the full coupling scheme: Panel (a) shows the initial condition, then after 3ms we see the propagation in the Purkinje fiber (panels (b, c)). Then, in panel (d) we see how the fiber activates the myocardium in the down left coupling region. After that, the electrical wave propagates through the myocardium (panels (e, f, g)). When the electrical wave arrives at the top right corner (panel (h)) it activates the second segment of the Purkinje (panel (i)).

In Figure 5, we show the plateau phase in panels (a,b) and the repolarization in panels c, d and e.

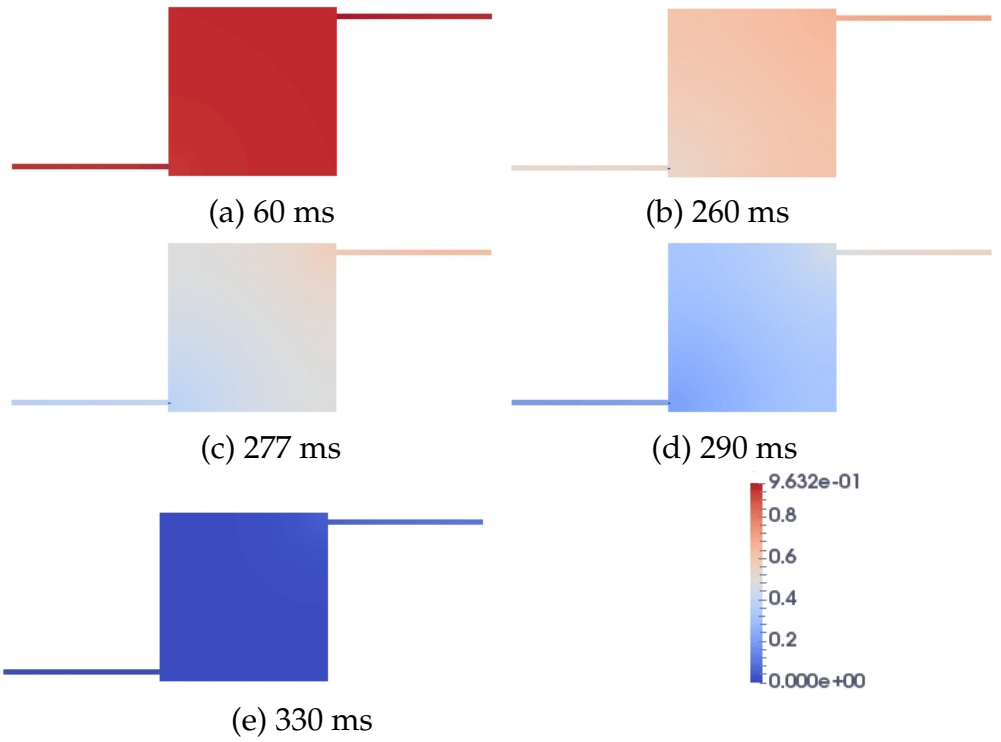

(a) 60 ms (b) 260 ms (c) 277 ms (d) 290 ms (e) 330 ms

Figure 5: Snapshots of the electrical potential at the plateau phase (panels (a,b)) and at the repolarization phase (panels (c,d,e)). The simulation is performed with the full coupling scheme.

5.2. Accuracy of the numerical schemes

In order to compare the different time-splitting schemes to the reference solution, we performed the three other simulations using the same model and discretization parameters as for the full coupling. In Figure 6 we present a snapshot the transmembrane potential at time 27 ms computed using the full coupling scheme (6a), the Purkinje to myocardium Gauss-Seidel scheme (6b), the myocardium to Purkinje Gauss-Seidel scheme (6c) and the Jacobi scheme 6d). One can see that the electrical wave reaches the top corner of the myocardium domain at the same time.

Since the coupled problem does not have an analytical solution, in order to study the time convergence of the numerical schemes, we first compute a reference solution using small space and time steps. After that, we compute the solution for each of the time-splitting schemes by dividing the time of the space step several times. For the time convergence, we compute our reference solution with $h = 5\times10^{-3}$ cm and $\Delta t = 0.0001$ ms. We compute the four solutions for $\Delta t = 0.1, 0.05, 0.025, 0.0125, 0.005, 0.0025$ and 0.001 ms using the same space discretization as the reference solution $h = 5\times10^{-3}$, in order to avoid mixing the space and time discretization errors. We denote by $(V_h, V_{\mathrm{p},h})^{\mathrm{ref}} = (V_h^{\mathrm{ref}}, V_{\mathrm{p},h}^{\mathrm{ref}})$

the couple of the transmembrane myocardium and Purkinje potentials for the reference solution. For each of the schemes, we compute the L^2 relative error as follows:

$$Error = \frac{\|(V_h, V_{\mathrm{p},h})^{\mathrm{ref}} - (V_h, V_{\mathrm{p},h})\|_{L^2((0,T)\times\Omega\cup\Lambda)}}{\|(V_h, V_{\mathrm{p},h})^{\mathrm{ref}}\|_{L^2((0,T)\times\Omega\cup\Lambda)}}, \tag{5.1}$$

where $\|(V_h, V_{\mathrm{p},h})^{\mathrm{ref}} - (V_h, V_{\mathrm{p},h})\|^2_{L^2((0,T)\times\Omega\cup\Lambda)} = \|V_h^{\mathrm{ref}} - V_h\|^2_{L^2((0,T)\times\Omega)} + \|V_{\mathrm{p},h}^{\mathrm{ref}} - V_{\mathrm{p},h}\|^2_{L^2((0,T)\times\Lambda)}$. The time grid used for the comparison with the reference solution is with $\Delta t = 0.1$ ms corresponding to the coarser time discretization.

In order to study the space convergence, the reference solution is computed with $h = 0.00125$ cm. The number of vertices in the reference solution mesh is equal to $801 \times 801 + 2 \times 801 = 643203$. We keep the time discretization as the reference solution, we vary $h = 0.1, 0.05, 0.025, 0.01, 0.005$ and 0.0025 cm, and we compute the relative error using the formula (5.1). In order to compute the comparison, all the solution are projected on the coarser mesh ($h = 0.1$ cm). Here we don't introduce any interpolation, since we use regular triangular meshes, the vertices of the coarse mesh are included in all of the other meshes.

In Figure 7 (left) (respectively, right), we show the convergence in time (respectively, space) for all the numerical schemes. We see that the four schemes are of order one in time (respectively, space). This is in line with space and time discretization used here. The uncoupling schemes do not alter the order of convergence. We also see that both Gauss-Seidel schemes are more accurate than the Jacobi scheme.

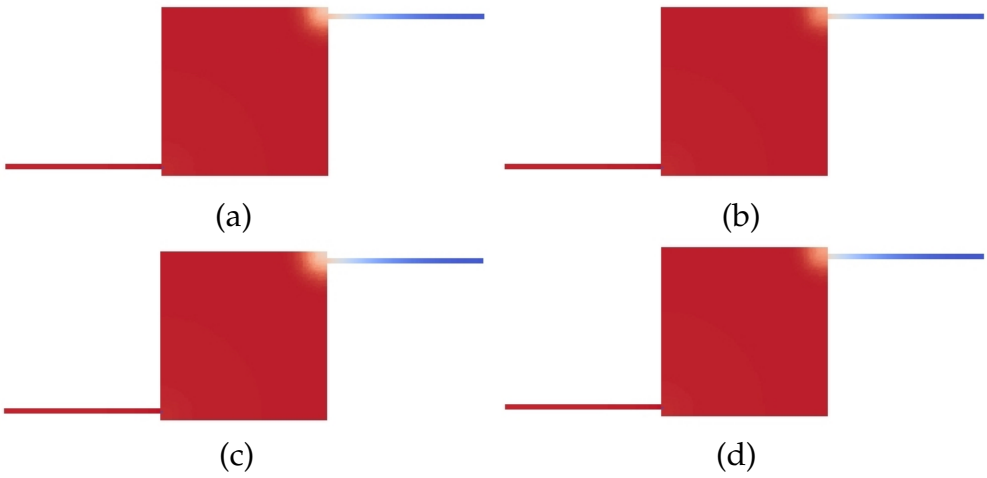

Figure 6: Snapshots of the action potential in the Purkinje and the myocardium domains at time 27ms: (a): full coupling scheme, (b):Gauss-Seidel scheme (Purkinje to myocardium). (c): Gauss-Seidel scheme (myocardium to Purkinje) and (d): Jacobi scheme.

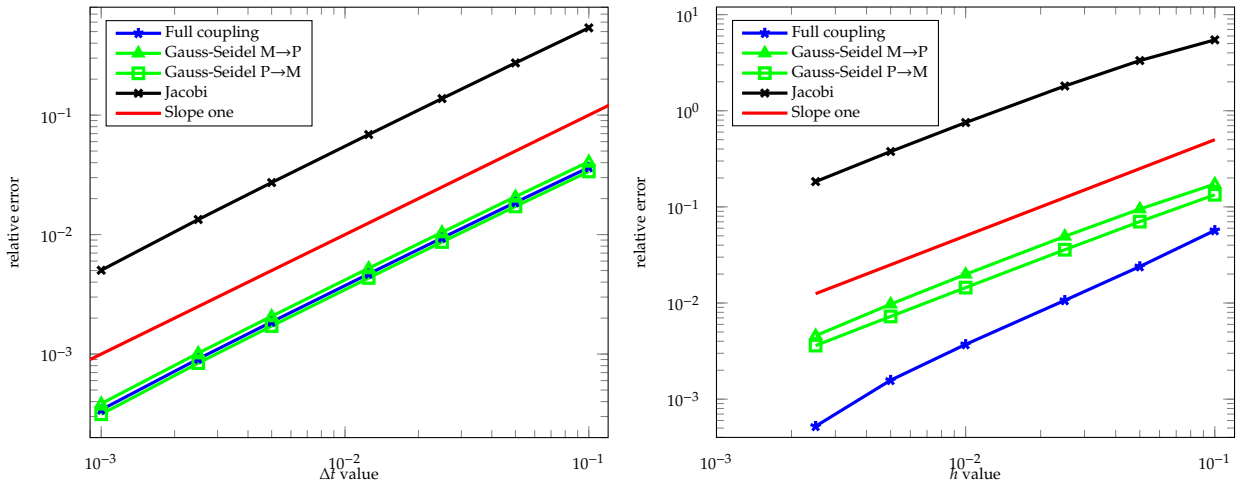

Figure 7: Time (left) and space (right) convergence of the transmembrane potential error for the full coupling, Gauss-Seidel and Jacobi time-marching schemes.

5.3. 1D-3D numerical results

In this paragraph, we use the previously described numerical schemes in a 1D/3D coupling framework. We also use physiological models for cell membrane ionic current description instead of the two state variable MS phenomenological model used for the mathematical analysis. The high non-linearity and the complexity of physiological models make the stability analysis for those models very technical and probably not possible using the same argument that we used for the phenomenological model. Thus, in this section, we only use the four schemes presented bellow to show that the uncoupling between the Purkinje and myocardium problem allow us to solve two symmetric positive definite problems instead of one non-symmetric problem without loss of accuracy.

5.3.1. Model setup

The heart domain is discretized using a 3D tetrahedral mesh as presented in Figure 8 (left). Due to the small scale of the His-Purkinje system, and its location within the ventricles, measurements of its anatomy are often not available. Thus we manually construct the Purkinje network on the realistic geometry of the heart Figure 8 (middle) representing left and right His bundles and simplified ramification of the Purkinje system. Each extremity of the Purkinje network is coupled to the ventricular domain. Each coupling regions (Ω_i), is given by a small bull with radius 3 mm, as shown in Figure 8 (right).

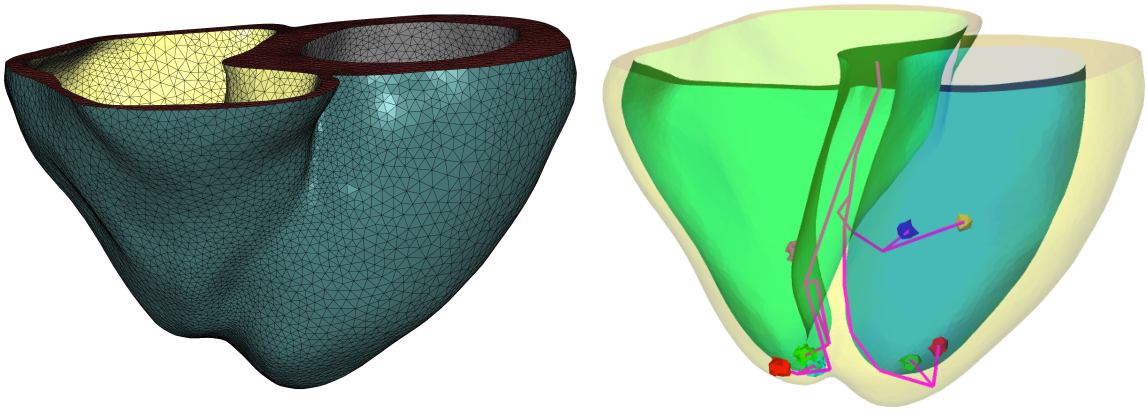

Figure 8: Space discretization of the Heart geometry (left). Purkinje system embedded in the heart geometry showing the coupling regions in the ventricles (right): Seven branching nodes and eight Purkinje/myocardium coupling regions.

We use the Ten Tusscher *et.al* model [33] for the ventricular domain and Difrancesco-Noble model [10] for the Purkinje network. For each of these two models, the ionic current is described using different ionic channels. For instance, the Ten Tusscher *et.al* model consists of 19 state variables used in order to describe 12 ionic currents. The total ionic current is given by

$$I_{\text{ion}} = I_{Na} + I_{K_1} + I_{to} + I_{Kr} + I_{Ks} + I_{CaL} + I_{NaK} + I_{NaCa} + I_{bNa} + I_{bCa} + I_{pK} + I_{pCa},$$

where I_{Na} is the late sodium current, I_{K_1} is the inward rectifier current, I_{to} transient outward potassium current, I_{Kr} is the potassium rapid delayed-rectifier current and I_{CaL} is the L-type calcium current. I_{NaCa} is the Na^+/Ca^{2+} exchanger current, I_{NaK} is Na^+/K^+ pump current, I_{pCa} and I_{pK} are plateau Ca^{2+} and K^+ currents. I_{bCa} and I_{bK} are background Ca^{2+} and K^+ currents. The full description of the ODE system and the expression of the different currents could be found in [33]. In this study case, we stimulate the Purkinje network at its free extremity located at the base of the heart, the electrical wave then propagates from Purkinje to the myocardium. At the branching nodes, we use the Kirchhoff law: That's the sum of the current flowing into the branching node is equal to zero. The values of the different parameters used in this simulation are given in Table 2. The parameter of the ionic models for both Purkinje and ventricular cells are those from the original papers [10] and [33] respectively. We use a first-order Rush-Larsen method for solving the ionic model. This numerical method has been successfully used for solving ionic models in cardiac electrophysiology [29, 24].

Table 2 Values of Purkinje and myocardium PDE model parameters

A (A_p)	C (C_p)	σ	σ_p	c_p	S_p
$10^3 cm^{-1}$	$10^{-3} mF/cm^2$	4 mS/cm	1 mS/cm	2 mS	0.04 cm^2

5.3.2. Full coupling simulation

In this paragraph, we show the numerical results of the coupling between the Purkinje network and the myocardium using the previously presented numerical schemes. First, we present the results for the full coupling scheme. As for the 2D case, this solution would be considered as the reference solution and would be compared later to the solutions of the other numerical schemes. We use a time step $\Delta t = 0.1$ ms. In Figure 9, we show the distribution of the transmembrane potential both in the Purkinje network and in the ventricles:

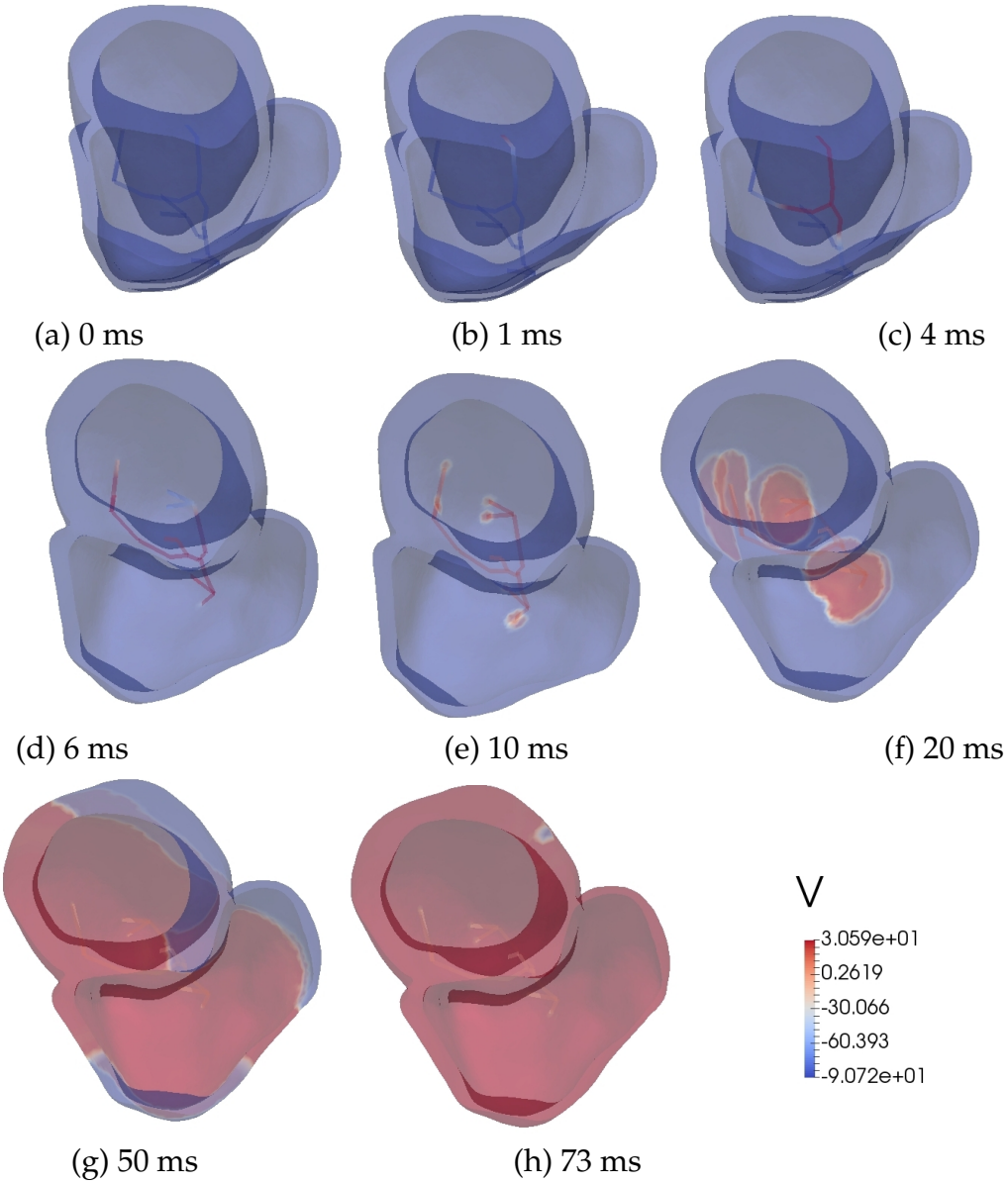

Figure 9: Snapshots of the depolarization phase of the electrical wave showing the circulation of the electrical wave from Purkinje to the myocardium. Simulations are performed with the full coupling scheme. The color bar shows the values of the electrical potential in mV.

At time zeros (panel a) the heart is fully repolarized, after stimulating the His bundle and the atrioventricular node located at the base of the heart, the electrical wave propagates in the one-dimensional domain (panel b) and through the branching nodes (panel c). The electrical wave achieves the terminal nodes at time 6 ms (panel d) and starts activating the ventricular cells in the coupling regions. All the coupling regions are activated at time

10 ms (panel e). Then the electrical wave propagates in the ventricles (panels f,g). The heart is fully depolarized at time 74 ms. We show in (panel h), the distribution of the transmembrane potential at time 73 ms where the heart is nearly full depolarized.

In Figure 10, we show the distribution of the transmembrane potential at the plateau phase (panels a,b) and at the repolarization phase (panels c, d). Since we did not introduce any heterogeneity in the ionic model making the distinction between the His bundle and the Purkinje network transmembrane potential, all the rapid conduction system have the same action potential duration (APD).

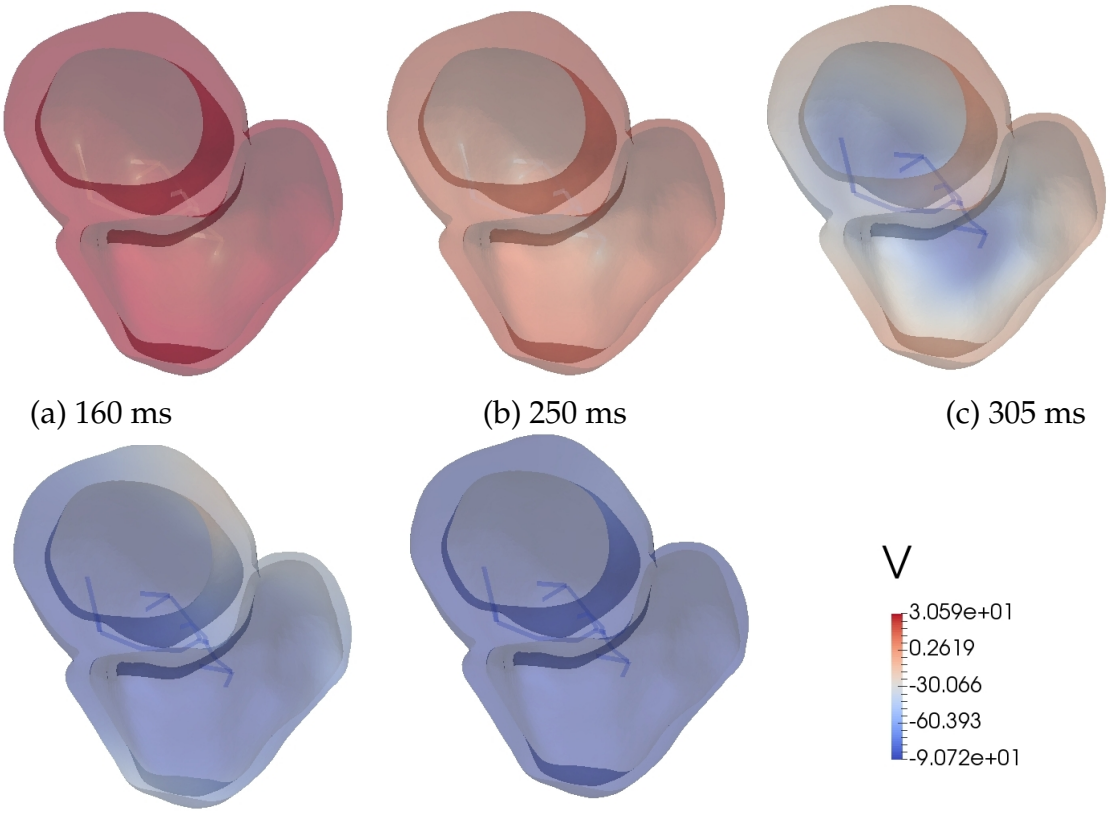

(a) 160 ms (b) 250 ms (c) 305 ms

(d) 335 ms (e) 360 ms

Figure 10: Snapshots of the electrical potential at the plateau phase (panels (a,b)) and at the repolarization phase (panels (c,d,e)). The simulation is performed with the full coupling scheme. The color bar shows the values of the electrical potential in mV.

The APD in Ten Tusscher model is higher than it is in the Difrancesco-Noble model: We can see at time 250 ms (panel b) that the Purkinje is repolarizing but the ventricular cells are still at the plateau phase. At time 305 ms (panel c), the Purkinje network is fully repolarized and the ventricular cells are not yet. The whole heart is fully repolarized at time 360 ms (panel e).

5.3.3. Comparison of the different numerical schemes

In this paragraph, we compare the solution of the times splitting schemes to the full coupling solution presented in the previous paragraph. First, we remark that in terms of the numerical stability all the time-splitting schemes have the same restriction on the time step size Δt. In Table 3, we show that all the numerical schemes are stable for Δt = 0.05, 0.1 and 0.15 ms and are not stable for Δt = 0.175 and 0.2 ms. This reflects CFL-like stability condition that we see in the Theorem 4.

Table 3 Stability sensitivity to the time step size Δt (ms). Symbol ✕ indicates numerical instability and symbol ✓ indicates numerical stability.

scheme / Δt (ms)	Coupled	Gauss-Seidel M→P	Gauss-Seidel P→M	Jacobi
0.05	✓	✓	✓	✓
0.1	✓	✓	✓	✓
0.15	✓	✓	✓	✓
0.175	✕	✕	✕	✕
0.2	✕	✕	✕	✕

Second, looking at the trace of the transmembrane potential at a given point in the Purkinje network Figure 11 (left), one could not distinguish the difference between the four studied schemes. In order to observe the differences in the traces, we made a zoom in of the transmembrane potential at the upstroke period from 5.995 ms to 6.025 ms. The differences are very negligible. In Figure 12, we show the time course of the transmembrane potential recorded at a given point at the left ventricle. The four numerical schemes provide visually indistinctive transmembrane potentials. Only, when zooming in at the repolarization phase for instance we distinguish the different traces.

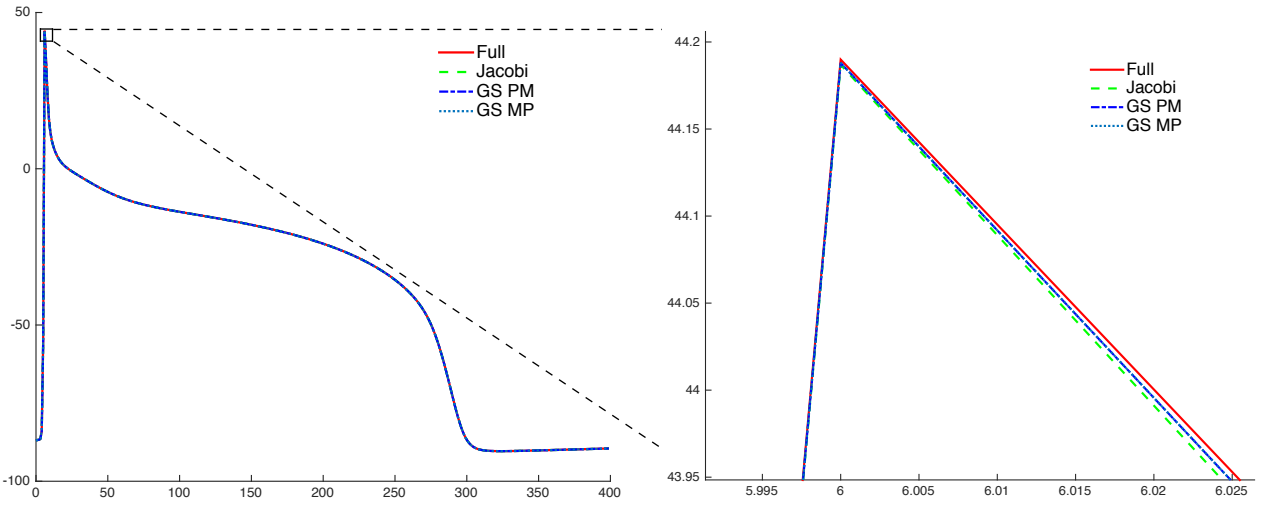

Figure 11: Comparison of the Numerical schemes on the Purkinje action potential trace at a given point in the Purkinje network: Full coupling (red continuous line), Jacobi scheme (green dashed line), Gauss-Seidel myocardium to Purkinje (blue dotted line) and Gauss-Seidel Purkinje myocardium (blue dashed line). X-axis: time (ms). Y-axis: electrical potential in mV.

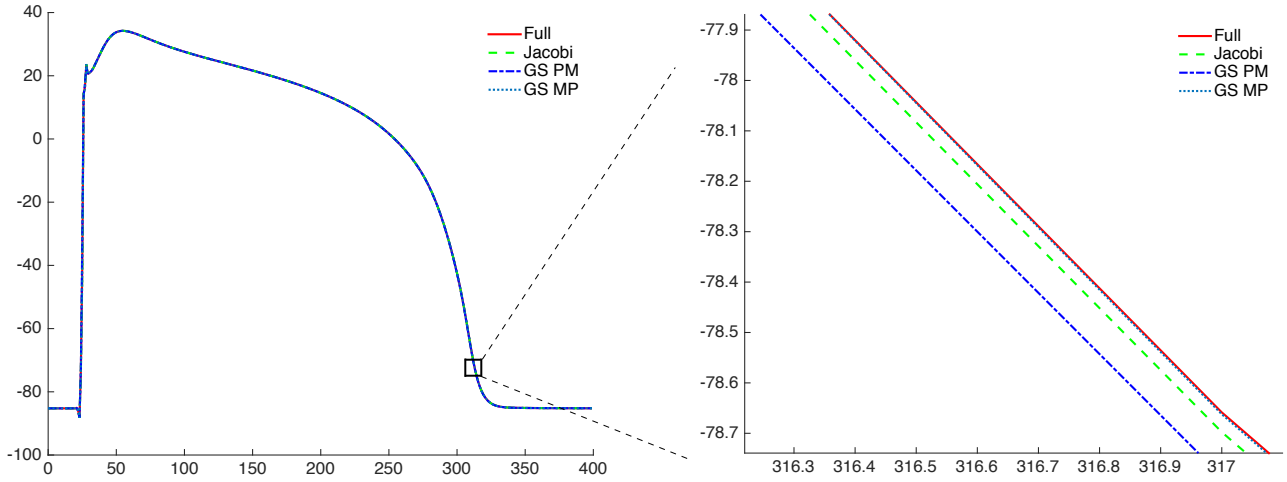

Figure 12: Comparison of the Numerical schemes on the myocardium action potential trace at a given point in the ventricles: Full coupling (red continuous line), Jacobi scheme (green dashed line), Gauss-Seidel myocardium to Purkinje (blue dotted line) and Gauss-Seidel Purkinje myocardium (blue dashed line). X-axis: time (ms). Y-axis: electrical potential in mV.

One of the main biomarkers used to compare two different simulations in cardiac electrophysiology is the activation map (the time when the cell is depolarized). Here we define the activation map as a function that for each point in space gives the time when the transmembrane potential reaches 0 mV. In Figure 13, we show the activation map for each of the solutions of the four schemes represented in a cut of the heart domain: In (panel a), respectively (panels b, c, d), we show the activation map of the full coupled problem, respectively (Gauss-Seidel M→P, Gauss-Seidel P→M, Jacobi) solution. The L^2 error of between the solutions obtained by the time-splitting schemes and the implicit coupling scheme are less than 0.2%.

(a) Full coupling

(b) Jacobi scheme)

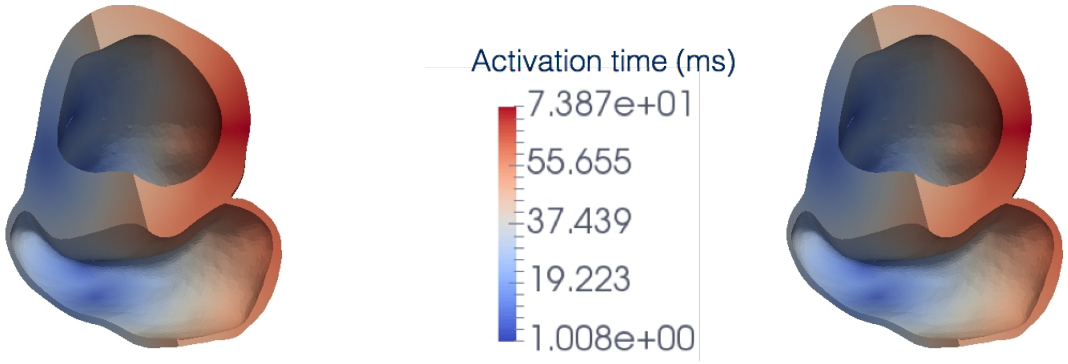

(c) Gauss-Seidel scheme (M->P

(d) Gauss-Seidel scheme (P->M)

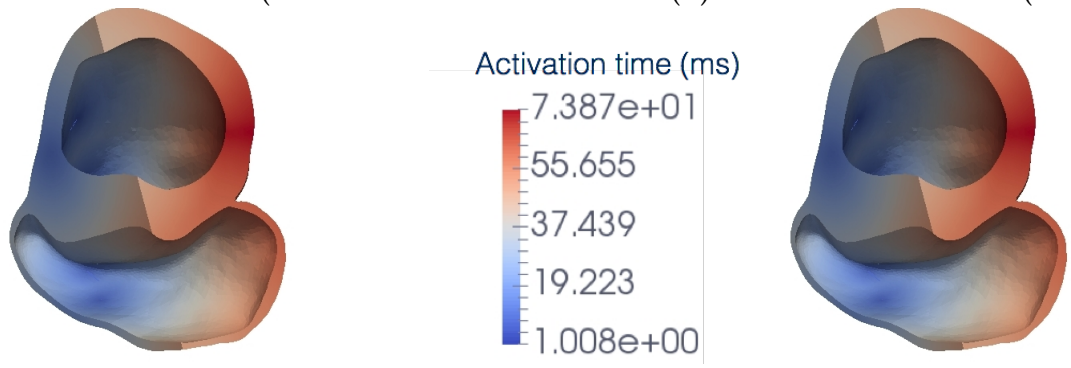

Figure 13: Comparison of the activation time maps obtained using the different numerical schemes. The color bar shows the values of the activation times in ms.

5.3.4. Retrograde Propagation

In this paragraph, we wanted to show the retrograde propagation of the electrical wave in the Purkinje system. This means that in this case, the electrical wave does not come from the atrioventricular node but comes from the ventricular muscle. In order to perform this simulation case, we stimulate the heart ventricles instead of stimulating the His bundle at the base of the heart. The retrograde propagation is known to be one of the main cause of polymorphic ventricular tachycardias and may lead to ventricular fibrillation [5, 15]. Here we performed a retrograde simulation where we stimulate the ventricular domain at the apex of the heart, the electrical wave then propagates through the ventricular domain and quickly reaches the PMJ regions as shown in Figure 14 (panel a). The electrical wave takes a long time to propagate from the myocardium to Purkinje, in our case, it took about 30 ms to activate the Purkinje system Figure 14 (panels b and c).

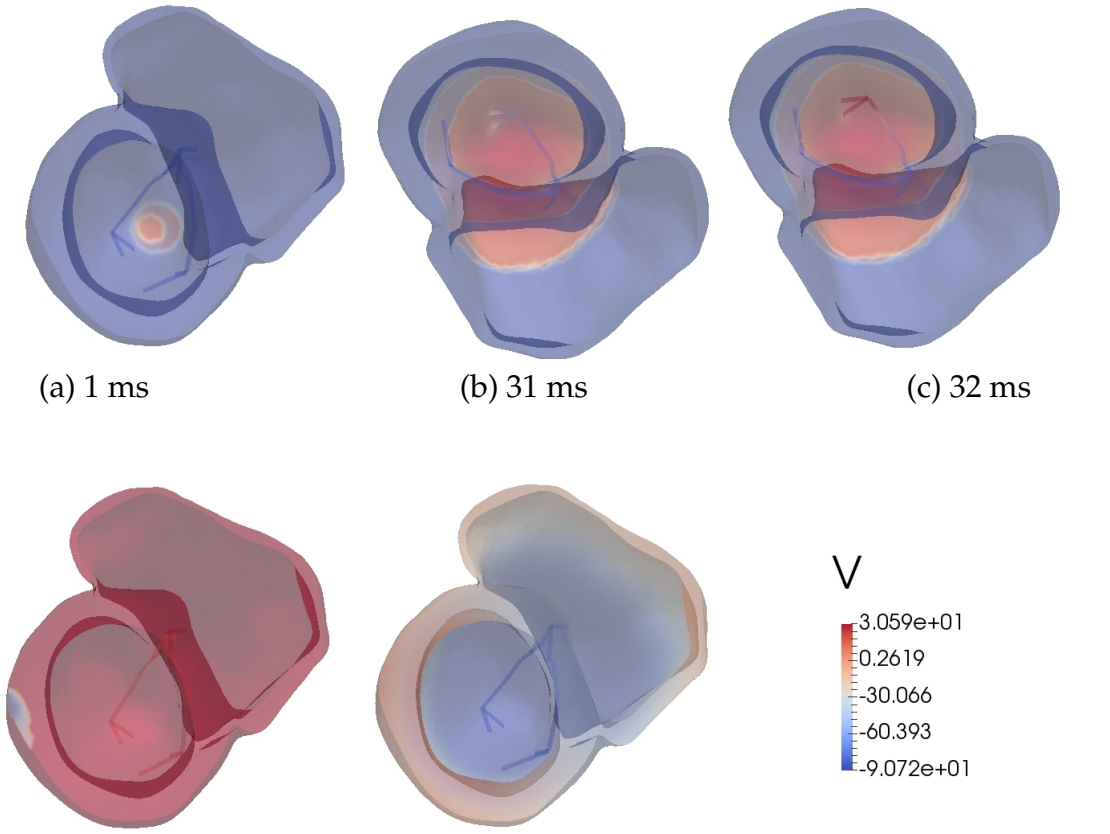

(a) 1 ms (b) 31 ms (c) 32 ms

(d) 77 ms (e) 280 ms (f) Color bar mV

Figure 14: Snapshots of the depolarization phase of the electrical wave showing the circulation of the electrical wave from myocardium to Purkinje. Simulations are performed with the full coupling scheme. The color bar shows the values of the electrical potential in mV.

6. Discussion and conclusion

In this paper, we demonstrated a theoretical result about the numerical stability of four different schemes allowing to solve the Purkinje myocardium coupled monodomain equations using the MS ionic model. The first theorem shows the stability at the semi-discrete level. The second theorem shows the stability of the four different numerical schemes at the fully discretized level. The first scheme treats the coupling problem in an implicit manner and the three remaining schemes provide different splitting schemes allowing to solve the PDE in the myocardium domain independently from the PDE in Purkinje system 1D domain. Results show that we do not need an additional restriction on the time step Δt in order to guarantee the stability of the time-splitting schemes. Both for the full coupling and the time-splitting schemes, we show that we have a CFL-like restriction of the time step $\Delta t = O((h))$. The results show also that time-splitting slightly alter the energy of the problem. These theoretical results were followed by numerical simulations. In order to show the convergence of the numerical schemes, we performed 2D/1D coupling simulations. These simulations illustrate the exactitude of the theoretical study. We show the convergence of the numerical solution by studying the error between a reference solution (obtained using the full coupling scheme with very refined space and time discretization) and the different uncoupling schemes: The relative error slightly altered by the Gauss-Seidel uncoupling schemes and more affected by the Jacobi scheme. The order of the convergence is the same for all the four schemes. We also performed 3D/1D simulations for the four studied schemes using a 3D realistic heart geometry and a manually constructed Purkinje system including His, left and right bundles and Purkinje fibers. We also used physiologically detailed ionic models for both myocardium and Purkinje cells. Although we did not prove the stability for the coupled problem using physiological ionic models, numerical simulations are coherent with the theoretical result obtained with the MS phenomenological ionic model and the numerical simulations obtained in the 2D case. In fact, 3D simulations show that the relative error between the fully coupled solution and the different time-splitting schemes are less than 0.2%. The different plots show that the uncoupling schemes do not alter the propagation of the electrical wave. The difference between the transmembrane solution obtained by the different numerical schemes is almost invisible when looking at the transmembrane potential traces of a heart beat. Only by zooming-in over a small time window that we could distinguish between them. We also performed a retrograde propagation simulation where we stimulate the heart in the myocardial domain in a region at the apex. We found that the electrical wave takes almost 30 ms in order to activate the Purkinje fibers. We think that this delay is related to the coupling parameters S_{p} the membrane surface of the Purkinje cells in the coupling region Ω_i and c_{p} the conductance of the Purkinje/muscle junction. Future works would concern the sensitivity of the coupled problem solution to those parameters but also to the pattern variabilities of the Purkinje network.

References

[1] Shimon Abboud, Omer Berenfeld, and Dror Sadeh. Simulation of high-resolution qrs complex using a ventricular model with a fractal conduction system. effects of ischemia on high-frequency qrs potentials. *Circulation research*, 68(6):1751–1760, 1991.

[2] Rubin R Aliev and Alexander V Panfilov. A simple two-variable model of cardiac excitation. *Chaos, Solitons & Fractals*, 7(3):293–301, 1996.

[3] Adnane Azzouzi, Yves Coudière, Rodolphe Turpault, and Nejib Zemzemi. A mathematical model of the purkinje-muscle junctions. *Mathematical biosciences and engineering: MBE*, 8(4):915–930, 2011.

[4] Go W Beeler and H Reuter. Reconstruction of the action potential of ventricular myocardial fibres. *The Journal of physiology*, 268(1):177, 1977.

[5] Omer Berenfeld and José Jalife. Purkinje-muscle reentry as a mechanism of polymorphic ventricular arrhythmias in a 3-dimensional model of the ventricles. *Circulation Research*, 82(10):1063–1077, 1998.

[6] Rafel Mark Bordas, Kathryn Gillow, David Gavaghan, Blanca Rodríguez, and David Kay. A bidomain model of the ventricular specialized conduction system of the heart. *SIAM Journal on Applied Mathematics*, 72(5):1618–1643, 2012.

[7] Marina Cerrone, Sami F Noujaim, Elena G Tolkacheva, Arkadzi Talkachou, Ryan OConnell, Omer Berenfeld, Justus Anumonwo, Sandeep V Pandit, Karen Vikstrom, Carlo Napolitano, et al. Arrhythmogenic mechanisms in a mouse model of catecholaminergic polymorphic ventricular tachycardia. *Circulation research*, 101(10):1039–1048, 2007.

[8] Yves Coudière and Charles Pierre. Stability and convergence of a finite volume method for two systems of reaction-diffusion equations in electro-cardiology. *Nonlinear analysis: real world applications*, 7(4):916–935, 2006.

[9] Carlo D'ANGELO and Alfio Quarteroni. On the coupling of 1d and 3d diffusion-reaction equations: Application to tissue perfusion problems. *Mathematical Models and Methods in Applied Sciences*, 18(08):1481–1504, 2008.

[10] Dario DiFrancesco and Denis Noble. A model of cardiac electrical activity incorporating ionic pumps and concentration changes. *Philosophical Transactions of the Royal Society of London B: Biological Sciences*, 307(1133):353–398, 1985.

[11] Marc Ethier and Yves Bourgault. Semi-implicit time-discretization schemes for the bidomain model. *SIAM Journal on Numerical Analysis*, 46(5):2443–2468, 2008.

[12] Cecilia Fantoni, Mihoko Kawabata, Raimondo Massaro, Francois Regoli, Santi Raffa, Vanita Arora, JORGE A SALERNO-URIARTE, Helmut U Klein, and Angelo Auricchio. Right and left ventricular activation sequence in patients with heart failure and right bundle branch block: a detailed analysis using three-dimensional non-fluoroscopic electroanatomic mapping system. *Journal of cardiovascular electrophysiology*, 16(2):112–119, 2005.

[13] Miguel A Fernández and Nejib Zemzemi. Decoupled time-marching schemes in computational cardiac electrophysiology and ecg numerical simulation. *Mathematical biosciences*, 226(1):58–75, 2010.

[14] Richard FitzHugh. Impulses and physiological states in theoretical models of nerve membrane. *Biophysical journal*, 1(6):445, 1961.

[15] Michel Haissaguerre, Edward Vigmond, Bruno Stuyvers, Meleze Hocini, and Olivier Bernus. Ventricular arrhythmias and the his-purkinje system. *Nature Reviews Cardiology*, 2016.

[16] Monica Hanslien, Kenneth H Karlsen, and Aslak Tveito. On a finite difference scheme for a beeler-reuter based model of cardiac electrical activity. *International Journal of Numerical Analysis and Modelling*, 3:395–412, 2006.

[17] John G Heywood and Rolf Rannacher. Finite-element approximation of the nonstationary navier-stokes problem. part iv: Error analysis for second-order time discretization. *SIAM Journal on Numerical Analysis*, 27(2):353–384, 1990.

[18] Ryo Imanishi, Shinji Seto, Shinichiro Ichimaru, Eiji Nakashima, Katsusuke Yano, and Masazumi Akahoshi. Prognostic significance of incident complete left bundle branch block observed over a 40-year period. *The American journal of cardiology*, 98(5):644–648, 2006.

[19] Karl Kunisch and Aurora Marica. Well-posedness for the mitchell-schaeffer model of the cardiac membrane. *SFB-Report No*, 18:2013, 2013.

[20] Gustavo Lopera, William G Stevenson, Kyoko Soejima, William H Maisel, Bruce Koplan, John L Sapp, S Dinakar Satti, and Laurence M Epstein. Identification and ablation of three types of ventricular tachycardia involving the his-purkinje system in patients with heart disease. *Journal of cardiovascular electrophysiology*, 15(1):52–58, 2004.

[21] Michel Lorange and Ramesh M Gulrajani. A computer heart model incorporating anisotropic propagation: I. model construction and simulation of normal activation. *Journal of electrocardiology*, 26(4):245–261, 1993.

[22] Ching-hsing Luo and Yoram Rudy. A model of the ventricular cardiac action potential. depolarization, repolarization, and their interaction. *Circulation research*, 68(6):1501–1526, 1991.

[23] Ching-hsing Luo and Yoram Rudy. A dynamic model of the cardiac ventricular action potential. i. simulations of ionic currents and concentration changes. *Circulation research*, 74(6):1071–1096, 1994.

[24] Megan E Marsh, Saeed Torabi Ziaratgahi, and Raymond J Spiteri. The secrets to the success of the rush–larsen method and its generalizations. *IEEE Transactions on Biomedical Engineering*, 59(9):2506–2515, 2012.

[25] Colleen C Mitchell and David G Schaeffer. A two-current model for the dynamics of cardiac membrane. *Bulletin of mathematical biology*, 65(5):767–793, 2003.

[26] Jinichi Nagumo, Suguru Arimoto, and Shuji Yoshizawa. An active pulse transmission line simulating nerve axon. *Proceedings of the IRE*, 50(10):2061–2070, 1962.

[27] Hong-Xia Niu, Wei Hua, Shu Zhang, Xin Sun, Fang-Zheng Wang, Ke-Ping Chen, Hao Wang, and Xin Chen. Assessment of cardiac function and synchronicity in subjects with isolated bundle branch block using doppler imaging. *Chinese medical journal*, 119(10):795–800, 2006.

[28] Denis Noble. A modification of the hodgkinhuxley equations applicable to purkinje fibre action and pacemaker potentials. *The Journal of Physiology*, 160(2):317, 1962.

[29] Mauro Perego and Alessandro Veneziani. An efficient generalization of the rush-larsen method for solving electro-physiology membrane equations. *Electronic Transactions on Numerical Analysis*, 35:234–256, 2009.

[30] Jack M Rogers and Andrew D McCulloch. A collocation-galerkin finite element model of cardiac action potential propagation. *IEEE Transactions on Biomedical Engineering*, 41(8):743–757, 1994.

[31] Kim Simelius, Jukka Nenonen, and Milan Horacek. Modeling cardiac ventricular activation. *International Journal of Bioelectromagnetism*, 3(2):51–58, 2001.

[32] Joel Smoller. *Shock waves and reaction?diffusion equations*, volume 258. Springer Science & Business Media, 2012.

[33] KHWJ Ten Tusscher, Denis Noble, Peter-John Noble, and Alexander V Panfilov. A model for human ventricular tissue. *American Journal of Physiology-Heart and Circulatory Physiology*, 286(4):H1573–H1589, 2004.

[34] KHWJ Ten Tusscher and Alexander V Panfilov. Modelling of the ventricular conduction system. *Progress in biophysics and molecular biology*, 96(1):152–170, 2008.

[35] Vidar Thomée. Galerkin finite element methods for parabolic problems second edition. *SPRINGER SERIES IN COMPUTATIONAL MATHEMATICS*, 25, 2006.

[36] Edward J Vigmond and Clyde Clements. Construction of a computer model to investigate sawtooth effects in the purkinje system. *Biomedical Engineering, IEEE Transactions on*, 54(3):389–399, 2007.

[37] Louis Wolff, John Parkinson, Paul White, et al. Bundle-branch block with short p-r interval in healthy young people prone to paroxysmal tachycardia. *Annals of noninvasive electrocardiology*, 11(4):340–353, 2006.